Potential of Flexible Carbon Nanotube Films for High Performance Strain and Pressure Sensors

Chapter · November 2014

7 authors, including:

Olfa Kanoun
Technische Universität Chemnitz
512 PUBLICATIONS **1,913** CITATIONS

SEE PROFILE

Abderrahmane Benchirouf
Technische Universität Chemnitz
29 PUBLICATIONS **230** CITATIONS

SEE PROFILE

Ayda Bouhamed
Technische Universität Chemnitz
21 PUBLICATIONS **195** CITATIONS

SEE PROFILE

Some of the authors of this publication are also working on these related projects:

GO sensor View project

Dirac Materials View project

6

Potential of Flexible Carbon Nanotube Films for High Performance Strain and Pressure Sensors

O. Kanoun[1], C. Müller[1], A. Benchirouf[1], A. Sanli[1], A. Bouhamed[1 2], A. Al-Hamry[1], and L. Bu[1]

[1]Technische Universität Chemnitz, Chair for Measurement and Sensor Technology, 09107 Chemnitz, Germany
[2]Higher Engineering School of Sfax (ENIS), University of Sfax, Sfax, postal code w.3038, Tunisia

Outline

Introduction

Strain sensors have a wide range of applications in engineering, industry and medicine for measuring different quantities, such as stress, torque, pressure and vibration. Despite their excellent features, conventional strain sensors, such as semiconductor and metallic strain gauges, show some limitations considering measurement range, low sensitivity, difficulties to be embedded in material structures, low fatigue life and sensitivity to environment conditions. These limitations increase the demands for using novel smart materials, e.g. doped silicon [1], nanoparticles [2-4], nanowires [5-6], graphene [7-9] and carbon nanotubes (CNTs) [10-14]. The different dimensions of carbon structures are exemplarily summarized in Figure 6.1. Among these materials, CNTs have become one of the most promising materials since their discovery by Iijima in 1991 [15] and they attracted a great interest in a wide range of fields because of their exceptional mechanical, electrical, thermal and chemical properties. The excellent properties of CNTs provide interesting opportunities to realize new types of strain gauges, which can overcome some performance limitations of conventional commercial metallic strain gauges and allow to enter in completely new application fields.
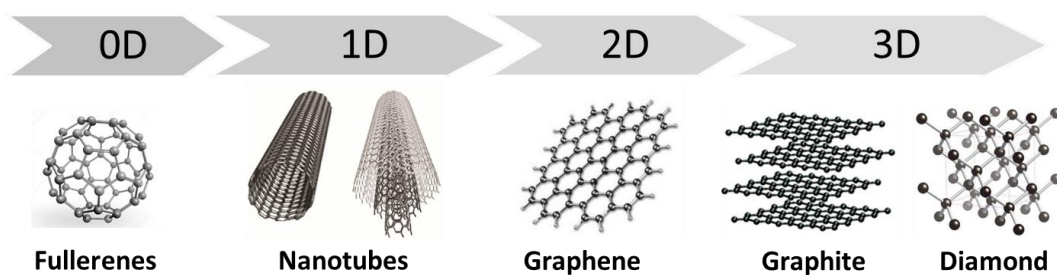

FIGURE 6.1
Crystal structure of carbon nanomaterials with different dimensions

In this chapter, we outline the flexible CNT films for high performance strain sensor and pressure sensors applications. This review is organized as follows. In section 2 the theoretical background about CNTs considering structure, electrical, mechanical and piezoresistive properties are introduced. Furthermore, in this section the fundamentals of percolation theory and the effect of nanofiller alignment on percolation threshold are also discussed. In section 3, we emphasize the strain sensor fabrication techniques and the working mechanism of CNT networks. The section 4 addresses the recent developments in strain sensors based on CNTs thin films, CNT/polymer composites and CNT yarns by considering the influence of the fabrication parameters, type of the CNTs and polymers on the strain sensor behavior and reproducibility. In section 5, current developments of pressure sensors based on CNTs and the influence of the process parameters, type of CNTs and polymer are discussed. In section 6 the potential of strain and pressure sensors for future applications is highlighted. We summarize in section 7 the most important results, which include limitations of current sensors and possible future developments towards flexible strain and pressure sensors.

Theoretical Background

Structure of CNTs

A single walled carbon nanotube (SWCNT) is the rolled-up form of a single graphene sheet. The rolling direction of a graphene sheet is described by the chiral vector $C_h = na_1 + ma_2$, where n and m are integers and a_1 and a_2 are the lattice vectors of graphene as illustrated in Fig. 6.2 [16]. SWCNTs can be in armchair, zigzag or chiral form depending on the integer values of n and m. The type of the chirality (n, m) is decisive for the physical properties of CNTs [16]. For instance, CNTs with "armchair" structure, where $n = m$, i.e. (n, n), have no band gap and therefore they are always metallic. In the case $m = 0$, i.e. $(n, 0)$ the structure is called "zigzag" where SWCNT can be either insulating or metallic. The SWCNT is metallic if $n = 3q$, where q is an integer. The third structure of SWCNT is called "chiral" where $n > m > 0$. The SWCNT with chiral structure can be metallic if $n - m = 3q$.

Multi walled carbon nanotubes (MWCNTs) consist of multiple rolled-up graphene sheets in two different structures called *russian doll model*, where graphene sheets are rolled up in concentric cylinders and in the *parchment model*, where one graphene sheet is rolled like a scroll of parchment [17]. MWCNTs are always metallic and their conductivity is quite complex due to the various coaxially arranged SWCNTs [18]. The electron transport in the MWCNTs is found to be similar with SWCNTs because most of the current passing through the tube is limited to the outermost layer [19,20].
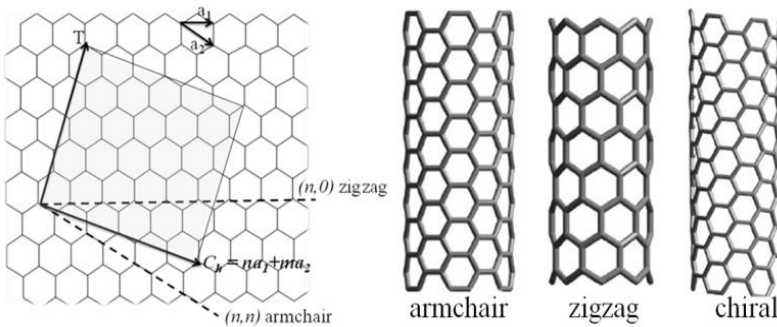

FIGURE 6.2
The construction of CNTs from a graphene sheet along the chiral vector C_h [16]

Mechanical Properties of CNTs

CNTs have a high stiffness and axial stress due to the covalent sp^2 hybridized bonding between carbon atoms [21]. Scientific measurements using in situ atomic force microscopy (AFM) and transmission electron microscopy (TEM) have been conducted to estimate the Young's modulus and it is in the range of 270 GPa to 950 GPa [22-23]. In comparison with conventional materials, CNTs show also high tensile strength of up to 63 GPa [24] due to extra energy absorption required for the hollow structures of carbon nanotubes. Mechanical properties of CNTs have a strong dependence on nanotube structural details such as; electronic band structure e.g. size dependent Young's modulus for small size SWCNT [25], tensile behavior dependence on helicity, diameter and defects. The effects of mechanical deformation i.e. kinking, sliding and compression were studied

both experimentally and theoretically by quantum mechanical simulations [26]. Mechanical tests inside a high resolution TEM were carried out by measuring the change of resistance of individual MWCNT when mechanically slided and kinked [27]. Tips from atomic force microscopy (AFM) were used to deflect suspended individual SWCNT and caused a decrease of two orders of magnitude of conductivity due to the formation of local sp^3 bonds between tube and tip [28]. When applying reversible deformations and compressive strains (bending) on individual SWCNTs with an AFM tip alterations of the band gap and the conductivity were observed [29]. A strain gauge was theoretically predicted by the tight-binding approach and for SWCNTs with diameter larger than 1 nm it was found to be chirality dependent [30].

Piezoresitive Properties of CNT Networks

Electromechanical and piezoresistive properties of randomly distributed CNT networks and CNT/polymer composites were studied experimentally and theoretically [31-34]. CNT/polymer composites have a percolation behavior where the interconnections between CNTs network form the conductive paths. The role of the polymer in the network is considered by the tunneling barrier i.e. the gap between neighboring tubes and tunneling barrier height. A box of three-dimensional statistical resistors network model using tunneling effect between neighboring nanotubes presents the CNT network. The overall network resistance consists of the resistance of the CNT filler and the tunneling resistance. In addition, capacitance is considered where a three-dimensional capacitance network, i.e. gap capacitance between neighboring tubes and capacitance between the electrodes by material, was also simulated and allowed studies in the frequency domain [32]. In numerical simulations a tunneling distance between neighboring CNTs was considered and Kirchhoff's current law and Ohm's law were applied to obtain the electrical current and conductivity. The piezoresistivity of the CNT network was influenced by three contributions, namely the conductive paths formed by CNTs, tunneling between neighboring CNTs and CNT piezoresistivity. Conductive paths and tunneling effects were found to play the major role on the piezoresistivity of the CNT network [31]. Further explanations with respect to CNT resistor network and tunnelling mechanism are given in section 5.

Percolation in CNT Networks and the Influence of Process Parameters on the Electrical Properties

A high sensitivity of strain measurement can be reached at the percolation threshold [10,31, 35]. The percolation threshold depends on different factors such as CNT aspect ratio, CNT type, shell quality, dispersion degree and the functionalization of the CNTs. Generally, CNT networks with functionalized CNTs have higher percolation thresholds than none functionalized CNTs. Numerous studies have shown that the percolation threshold and conductivity depend strongly on the polymer type, fabrication parameters, aspect ratio of CNTs (Fig. 6.3), disentanglement of CNT agglomerates, uniform spatial distribution of individual CNTs and degree of alignment [22, 36]. Therefore, percolation thresholds ranging from less than 0.5 wt% to over 10.0 wt% of CNTs loading have been observed experimentally [37-39]. It is expected that the addition of CNTs to a polymer significantly enhances the conductivity of the composite. In general, the electrical conductivity of heterogeneous systems above the percolation threshold can be described by a scaling law [40,41]:

$$\sigma = \sigma_0 (\theta - \theta_c)^t \qquad (1)$$

where θ is weight fraction of the conducting filler, θ_c corresponds to the percolation threshold, and t refers to the critical exponent. According to the percolation theory, the critical exponent depends only on the dimensionality of the system, i.e $t=1.6$ for two and $t=2$ for three dimensions.
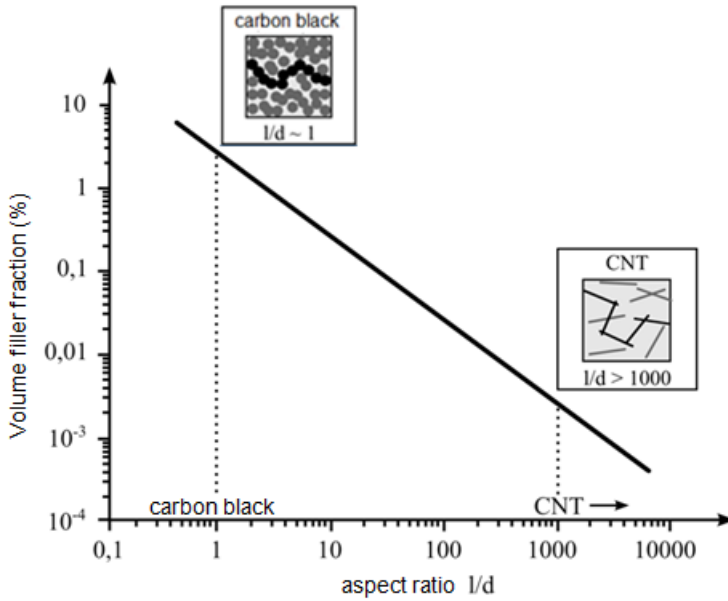

FIGURE 6.3
Volume filler fraction as a function of the aspect ratio *l/d* (length/diameter) exemplarily shown for carbon black and CNTs, redrawn from [38]

Wang et al. [42] dispersed two different kinds of MWCNTs (non-functionalized and COOH functionalized MWCNTs) with the same dimensions in silicon rubber, and he found that functionalized MWCNTs samples had four times higher resistance than non-functionalized MWCNTs.

In case of non-functionalized CNTs with an aspect ratio of 1000, Bauhofer and Kovacs [36] showed that the percolation threshold might be obtainable at 0.1wt% for nearly any optimized CNT/polymer composite. Above a concentration of 2 wt%, the conductivity reaches the saturation level (Fig. 6.4) [43].
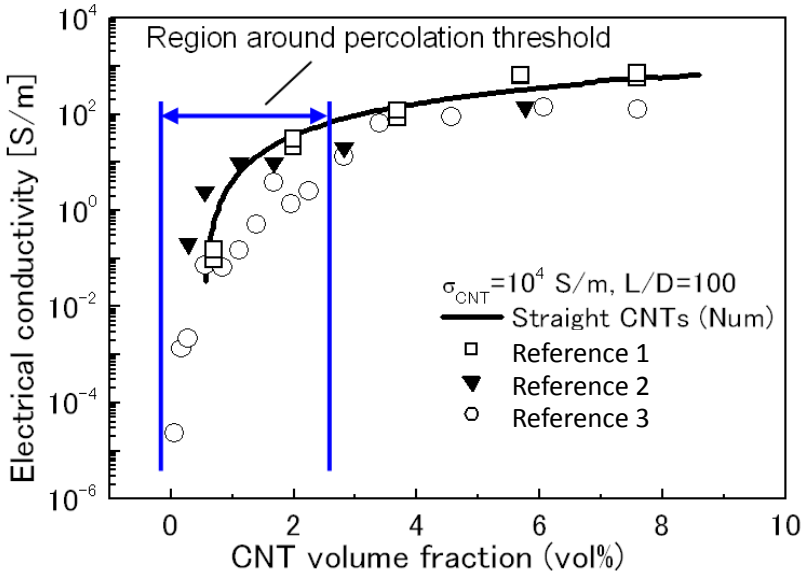
FIGURE 6.4
Electrical conductivity as a function of CNT volume fraction [43]

An important aspect especially for the fabrication is the step gradient of viscosity above the percolation threshold. A relationship between viscosity and conductivity was reported by Bauhofer et al. [36]. Alignment of CNTs in the composite can help to achieve low percolation thresholds. Grossiord et al. [44] reported a high conductivity of 1000 S/m for aligned MWCNTs (2 wt%) in polystyrene. Avilés et al. [45] aligned MWCNTs in polysulfon by applying alternating electrical fields E_{AC} of 6 kV/m and 7.3 kV/m. At low CNT concentrations (0.1 wt% – 0.5 wt%), the conductivity of the aligned composite was up to five orders of magnitude higher than that of randomly distributed CNTs. However, the conductivity was similar at higher CNT concentrations (0.75 wt%). Aligned MWCNTs showed a linear behavior of conductivity over the whole measurement range (Fig. 6.5(a)), whereby the randomly distributed CNTs showed two different regions (Fig. 6.5(b)) [45].
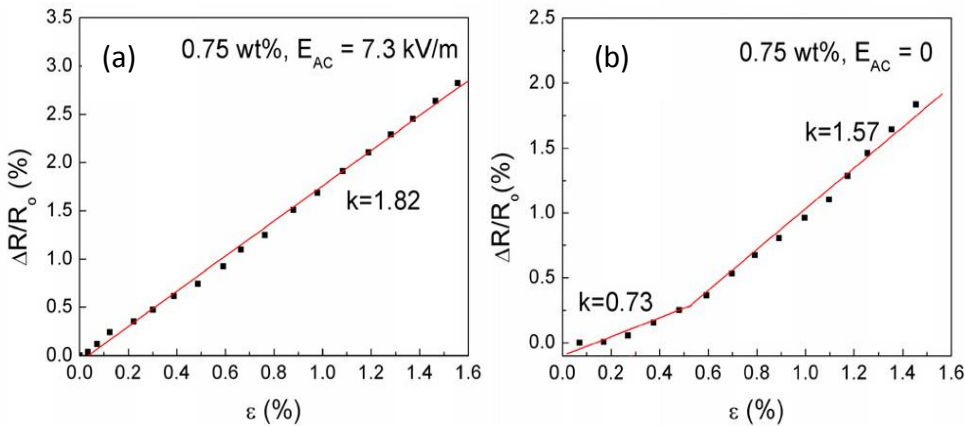

FIGURE 6.5
Piezoresistive characterization of MWCNTs/Polysulfone films. a) 0.75% MWCNTs, E_{AC} = 7.3 kV/m (aligned). b) 0.75% MWCNTs, E_{AC} = 0 kV/m [45]

Fabrication of Strain and Pressure Sensors

Preparation of CNT Dispersions and CNT/Polymer Composites

Agglomerates in nanocomposites deteriorate their electrical and mechanical properties and decrease their homogeneity, therefore realization of dispersion is a decisive step in the fabrication of CNT composites, especially for the realization of reproducible CNT-based structures with predictable properties. In general, CNTs have a mixture of various chiralities, diameters, lengths and defects. CNTs have a high aspect ratio and large surface areas, therefore they tend to assemble into bundles due to the Van der Waals attractive force between tubes [34]. CNTs are also hydrophobic and they have poor solubility in aqueous solutions and organic solvents [46].

Several processing methods are possible for fabricating CNT films and CNT/polymer composite films based on aqueous dispersions or polymer composites. The use of different polymers, such as thermoplastic, thermoset and elastomer matrices has been reported [47–49]. They mainly include methods to individually and homogeneously disperse CNTs within a solvent or polymer matrix [36,50–52] such as solution mixing, melt mixing, bulk mixing and *in situ* polymerization or combinations of them. In this section we address relevant processing techniques for both aqueous and polymer based dispersions.

Functionalization of CNTs

Covalent bonding of functional groups to the sidewalls and ends of CNTs can be achieved by chemical functionalization. This process can be performed with reactive molecules, such as fluorine, hydrogen, radicals, or aromatic cycles. Defect functionalization is another approach for covalent functionalization of CNTs. Defect sites are open ends, holes or deviations from the hexagonal graphene framework. The defect sites on CNTs, which can be created by strong oxidants such as HNO_3 or H_2SO_4, are stabilized with carboxyl or hydroxyl groups, allowing further chemical modifications and improved solubility of the CNTs in hydrophilic solvents. However, chemical functionalization and the corresponding preparation steps induce many defects, which are detrimental to the mechanical properties of the CNTs. Therefore, non-covalent or physical functionalization methods have been developed to disperse CNTs. Besides the wrapping with polymers, various non-ionic surfactants, such as polyoxyethylene octylphenylether (Triton X-100) [53]; anionic surfactants, such as sodium dodecylsulfate (SDS) [54], sodium dodecyl benzene sulfonate (SDBS) [55,56]; and cationic surfactants, such as dodecyl trimethyl ammonium bromide (DTAB) [57] have been employed for physical functionalization. In [55], it was proved than when using SDBS as surfactant higher percentages of single tubes could be obtained than when using SDS and Triton X-100 [55], and by by using optical spectroscopy [56]. Generally, ionic surfactants are preferable for dispersing CNTs in aqueous solutions and nonionic surfactants are suitable for dispersing CNTs in organic solvents [58]. The efficiency of the dispersion depends strongly on the properties and concentrations of solvent, CNTs and polymers.

Solution Mixing

The most common method to disperse CNTs and to fabricate CNT/polymer composites is solution processing. In general, the fabrication method includes the dispersion of CNTs in a solvent medium by mechanical mixing, magnetic stirring or sonication, mixing the CNT dispersion with the polymer solution and evaporation of the solvent. Surfactants are very important for dispersion of carbon

nanotubes. The interaction between CNTs and dispersion differs significantly depending on the chemical composition and concentration of the surfactant. For the dispersion of CNTs it is assumed that the minimum surfactant concentration below the critical micelle concentration is necessary in order to realize uniform and stable dispersions [61].

The mechanical treatment of the CNT solution is very important for the dispersion quality. The duration of mixing processes and the concentration of the surfactant influence the dispersion quality and the quantity of remaining agglomerates. Better unbundling is generally achieved by a higher surfactant concentration and longer processing times within a certain range. However, too intensive mechanical processing may lead to changes of the CNTs and introduce more defects. A high surfactant concentration leads to more residuals after drying processes, which influence the electrical properties of composite films. Therefore a compromise between surfactant concentration and processing time is required to achieve good unbundling. Furthermore, centrifugation processes are used to remove remaining CNT bundles.

In-situ Polymerization

In-situ polymerization of vinyl monomers in the presence of CNTs has been intensively studied for the fabrication of functional composites. This technique produces polymer-grafted CNTs mixed with free polymer chains [60]. Due to the small size of the monomeric molecules, the homogeneity of the composite is much higher than that obtained by mixing CNTs and polymer chains. In this sense, the method is suitable for the preparation of composites with enhanced mechanical properties due to strong interfacial bonds. Initially, *in-situ* radical polymerization has been successfully used for the synthesis of PMMA composites [61]. A combination of both *in-situ* polymerization and solution mixing is a promising approach for fabrication of polydimethylsiloxane (PDMS) composites. A generalized approach of this fabrication process is summarized in Figure 6.6.
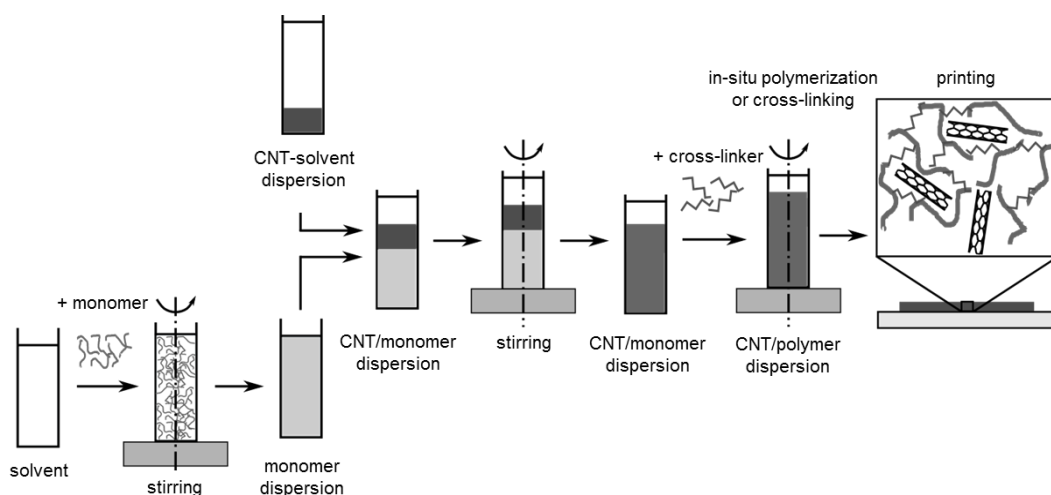

FIGURE 6.6
Fabrication of CNT/polymer composites using a combination of in-situ polymerization and solution mixing, adapted from [38]

Melt Blending

Thermoplastic polymers, such as polypropylene (PP) [62] or polystyrene (PS) [63], soften when heating above their melting point and can be utilized as matrix for CNT-based polymer composites. By blending the polymer melt with CNTs high shear forces are applied leading to a better homogeneity of the composite. Depending on the final morphology and shape of the composites, the samples can be further processed by several techniques, for example, extrusion or spinning [58]. Compared with composites prepared by solution mixing, the degree of dispersion of CNTs achieved by melt processing is lower and the fabrication is limited to small amounts of CNTs. Melt processing has the advantage that it can be used for insoluble polymers which cannot be processed with solution mixing.

Alignment of CNTs

In all the aforementioned cases, CNTs were randomly orientated within the composite. The utilization of CNTs within a polymer matrix strongly depends on the spatial distribution of the CNTs and the interactions at the interfaces. To bring the mechanical and physical properties of individual CNTs to the macroscopic level it is attractive to align CNTs in a certain direction. An efficient way to fabricate composites with aligned CNTs is based on the CVD growth of CNT and subsequent spin coating of a curable polymer on the as-grown nanotubes [64]. Alignment of CNTs in a dispersion or composite can be achieved by application of electric fields (dielectrophoresis) [65], magnetic fields [66] and mechanical forces [67]. In particular, dielectrophoresis has the potential for the fabrication of CNT based devices on the wafer-level. This method can be performed at room temperature and the process parameters such as alternating current, amplitude, frequency, and deposition time can tuned to optimize the alignment of CNTs. Fiber production techniques are also promising for fabricating aligned CNTs within a polymer matrix with excellent mechanical properties. Apart from melt spinning, solution based methods such as, coagulation spinning [68], gel spinning [69], dry-jet wet spinning [70] and electro-spinning [71] have been used for the fabrication of composite-based fibers.

Deposition of CNT Films and CNT/Polymer Composites

Deposition is required to transfer the dispersion onto a desired substrate. The film quality depends on rheological properties of the composite, the substrate material, the surface pretreatment and the properties of the deposition technique itself. The deposition process influences adhesion, force transfer and uniform force distribution within the film. Various deposition techniques, such as drop casting, layer by layer, inkjet printing, spin coating, spray coating, vacuum filtration and Meyer rod coating can be used to deposit CNT films. The most important film deposition techniques are shown in Fig. 6.7. In this section selected methods are briefly discussed. It should be noted that the development of nanocomposites is a growing field and therefore the number of deposition methods will be increasing in future.
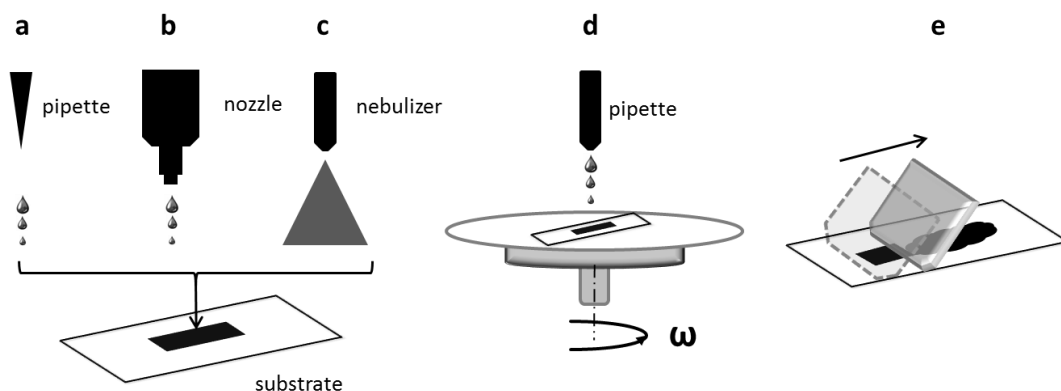
FIGURE 6.7
Selected deposition techniques for the fabrication of CNT and CNT/polymer films: a) Drop casting. b) Inkjet printing. c) Spray coating. d) Spin coating. e) Mayer rod coating/screen printing

Drop Casting

Drop casting is a simple and cheap technique to fabricate CNT films. Normally the prepared CNT dispersion is casted into a masked structure. After the evaporation of the solvent, the CNT film is formed and adhered to the substrate surface due to the van der Waals forces [72]. Changing the CNT concentration, the volume of the CNT dispersion and the number of deposited layers can control the thickness of the fabricated CNT film. By using drop casting, large area CNT films can be realized. The thickness of the generated CNT films typically spans several hundred nanometers to several micrometers [72]. The reached homogeneity of the CNT films with drop casting technique is limited. Due to the differential evaporation rates of the solution with dispersed particles, the so called "coffee ring effect" is often observed.

Layer-by-Layer Deposition

The layer-by-layer (LBL) self-assembly technique uses attraction forces such as electrostatic hydrogen bonding between the deposited species to deposit thin films onto the desired substrate. The thin films are fabricated by an alternative immersion of the substrate into two oppositely charged electrolytes (anionic and cationic) with a washing step in between. Thin films of a few nanometer can be reached. A higher film thickness could be realized by repeating these coating steps. This simple deposition technique is very powerful as it gives the ability to assemble complex structures on the nano-scale range at low costs [73-78].

Inkjet Printing

One of the potential advantages of solution-processed CNTs is the possibility of implementing inkjet printing to enable high-throughput large-area fabrication. In recent years, many researchers have investigated inkjet printing as a new deposition method to fabricate CNT films [79–81]. Different printing technologies to deposit CNTs on various substrates were subject of investigation, such as aerosol printing [82–84], screen printing [85] and contact printing [86]. Results show that using printing techniques has potential for fabricating low cost CNT devices and sensors [79]. By

inkjet printing macroscale structures can be directly patterned on substrates without the use of masks, photolithography and etching processes. In addition, various substrates can be used in the printing process, for example paper, polymer film, glass, wafer, and ceramic. Several investigations have shown promising results demonstrating the use of inkjet printing to fabricate CNT based flexible electronics [84,87–91]. Both organic solvent-based carbon nanotube inks [89–92] and water-based carbon nanotube inks with the use of dispersants have been developed [93–95]. Kordas *et al.* [79] reported large-area patterning of CNTs on paper and on polymers using a commercially available inkjet printer. In [81] SWCNTs, MWCNTs and functionalized CNTs were used to produce inks by mixing with the conductive polymer poly(3,4-ethylenedioxythiophene) (PEDOT). A piezoelectric inkjet printer was used to generate patterns on polymer films. Various printing parameters, such as voltage, frequency, drop spacing, substrate temperature and nozzle temperature were studied. Sheet resistances of the printed patterns were measured and compared with each other. The results indicated that functionalized CNTs are the best candidate to prepare the conductive CNT ink. By using functionalized CNTs (CNT-PEG) together with PEDOT-PSS [50:50] the lowest sheet resistance (225 Ω/sq) was achieved [81]. There are still some obstacles to the use of this deposition method, for example, nozzle clogging due to the presence of CNT agglomerates in the ink, relative slow speed and the microscopic inhomogeneity caused by the coffee ring effect that still has to be investigated.

Spin Coating

Spin coating is a technique for CNT film deposition and it is preferable for coating thin CNT films in the range of a few nanometers to hundreds of nanometers [96–98]. In contrast to other methods the film thickness can be easily controlled by the speed and coating time, various substrates can be used and the coating process can be performed at room temperature.
Kim *et al.* [98] used spin-coated dispersions of SWCNTs dispersed on glass substrates and achieved transparent and surfactant free SWCNT films, which have a root-mean-square roughness of 2.0 nm measured by AFM and a sheet resistance of 128 Ω/sq.

Spray Coating

Spray coating is similar to spin coating. It can be also used to deposit CNT films on various substrates up to large sizes. This deposition technique has been adopted to fabricate functional CNT devices [98–101]. However, spray-coated films have a higher roughness than those deposited by using spin coating [98].

Other Deposition Methods

Vacuum filtration and Meyer rod coating were reported in different studies [102–105]. Vacuum filtration has the advantage that the thickness of the filtrated CNT films can be easily controlled by the concentration and the volume of the CNT in the dispersion. The drawbacks of this technique are the limited film size of the filter and the necessity to transfer the films to more suitable substrates [103]. Meyer rod coating is another widely used deposition process for the fabrication of CNT films, because of its simple use for industrial mass products [104]. To apply Meyer rod coating defined rheological properties of the CNT dispersion are required.

Resistance of CNT Films and Strain Measurements

In order to understand the electrical conduction mechanism of the CNT film, the changes of the whole CNT network under strain have to be considered. In fact, not all CNTs within a CNT film contribute to the electrical conduction. The conductance of the CNT film is induced by the CNT network, which forms conducting paths between the electrodes. If each CNT in the film is assumed as a straight stick, the two-dimensional stick percolation theory [105] helps to reveal the electrical conduction mechanism of composites consisting of CNTs and an insulating matrix. When the conducting filler content is gradually increased, the composite undergoes an insulator-to-conductor transition. The critical filler content is referred as the percolation threshold where the electrical conductivity of the composite sharply increases several orders of magnitude due to the formation of conducting paths. Consequently, at the percolation threshold the sensitivity of the strain sensor is high. Below the percolation transition range, such conducting paths do not exist and the electrical properties are dominated by the matrix material. At filler amounts above the percolation transition range, multiple conduction paths exist and the electrical conductivity of the composite achieves a saturation level. When the composite is under strain, the configuration, position and orientation of the CNTs in the network change, that leads to significant modification of the conducting paths. In addition, the geometry and the area of the CNT film change also under applied strain. All these factors interplaying together lead to the film resistance changes under strain.

A CNT film can be seen as a network formed by a large number of randomly arranged individual CNTs and small CNT bundles. Two types of resistances determine the resistance of a CNT film. The first type is the intrinsic resistance R_{tube} of the CNT itself. Typical values for R_{tube} of MWCNTs are in the range of 0.2 kΩs/μm to 0.4 kΩs/μm. The second type is the intertube resistance $R_{junction}$. Then the total resistance of the CNT film can be calculated as:

$$R = R_{tube} + R_{junction} \qquad (2)$$

The part $R_{junction}$ can be further divided into the contact resistance R_C for CNTs in physical contact, and tunneling resistance R_T for CNTs separated by a small gap. The tunneling resistance R_T can be estimated by [106]:

$$R_T = \frac{h^2 d}{Ae^2 \sqrt{2m\lambda}} e^{\frac{4\pi d}{h}\sqrt{2m\lambda}} \qquad (3)$$

where d is the distance between CNT, e is the quantum of electricity, h is the Planck constant, m is the electron mass, λ is the barrier height of energy and A is the cross sectional area of the tunnel. From eq. (3) can be seen, that R_T increases nonlinearly, resulting in a nonlinear piezoresistivity.

The working mechanism in piezoresistive CNT strain sensors was mainly attributed to (i) variation of conductive CNT networks or loss of contacts among CNTs, affecting R_C, (ii) distance change between neighboring CNTs, promoting R_T and (iii) deformation of CNTs themselves, varying R_{tube}. However, due to poor stress transfer from the polymer matrix to the CNTs the contribution of R_{tube} to the piezoresistivity of the CNT strain sensor is expected to be very small. Hu et al. [107] used a combined 3D resistor network and fiber reorientation model to explain the working mechanism in piezoresistive CNT networks. They found that under low strains the resistance of composites with

CNT concentrations (< 1%) close to the percolation theshold is dominated by the tunneling effect instead of breakup of electrical contacts. At high CNT concentrations the piezoresitivitity was found to be almost linear. CNT networks within a composite or film also dominate the resistance-temperature behavior. The temperature response of a CNT network can be described based on a modified Lutinger liquid model and Fermi liquid theory by:

$$R(T) = R_{tube} T^{-\alpha} + R_{junction} T$$

(4)

where α is a constant value and T is the temperature [108].

When a CNT film is under strain, the change in the film resistance is the result of changes in both R_{tube} and $R_{junction}$. The change in R_{tube} under strain is due to the variation of the band-gap of individual tubes. This effect depends therefore on the chirality of individual tubes and has an exponential behavior with the strain [109]. Under stress, $R_{junction}$ changes with the varying inter-tube distances. Thereby, both contact and tunneling resistance change. This effect depends on the length and concentration of CNTs. Especially in the region of the percolation, the changes of $R_{junction}$ are more dominant in comparison to changes of R_{tube}.

In spite of significant investigations [110,111], fundamental understanding of the piezoresistive behavior in CNT/polymer composites still needs to be investigated. The total sensitivity of a piezoresistive CNT film can be quantified using the gauge factor K, which is defined as the relative change in electrical resistance with respect to the strain:

$$K = \frac{l}{\mathrm{d}l} \frac{\mathrm{d}R}{R}$$

(5)

where $\mathrm{d}R/R$ is the relative change in the resistance, generated by the applied strain $\varepsilon = \mathrm{d}l/l$. The K factor for CNT films can go up to 80 [30]. For classical metallic conductors (copper, nickel), this K factor is typically around 2. This high value of K for CNT films can be explained by two factors: the change of geometry of the sensor and the change in the percolation network of the system. Aforementioned points are very important for increasing the resolution of strain measurement, even by using low cost electronic components and AD-converters.

CNT and CNT/Polymer Strain Sensors

In order to overcome the limitations of conventional strain gauges, optimization of the fabrication parameters is crucial for the quality of the CNT based strain sensors. Depending on the sensor applications, there are some certain parameters, i.e. stability and repeatability that need to be fulfilled by the sensor prior to its practical use. It has been reported that the resistance of CNT/polymer film strain sensors change after a period of time under no mechanical load [17,4]. Moreover, CNT composite strain sensors show hysteresis in a cyclic strain loading [18-19]. In this section, the influence of process parameters such as sonication time, CNT type and temperature on the performance is shown. In addition, the behavior of both aligned and randomly distributed CNTs films in CNT yarns and CNT/polymer nanocomposite strain sensors are discussed.

CNT Film Strain Sensors

Early studies on the realization of the CNT based strain sensors are the fabrication of CNT films also called "Buckypapers" (BP) that have been reported in [10,104,110,111]. The buckypapers are mostly fabricated by dispersing CNTs in a solvent using a certain surfactant. Li et al. [110] reported about the piezoresistive effects of pristine SWCNTs thin films under strain at 19 ˚C. Gauge factors of up to 65 were achieved when applying up to 500 microstrains. Dharap et al. [104] investigated the potential and effectiveness of the SWCNT buckypapers for the multi-directional strain measurement at the macro scale for the measurements of structural surfaces. He fabricated the buckypapers by mixing unpurified SWCNTs with *N, N*-dimethylformamide (DMF) and then filtered the mixture by a Teflon membrane. The results showed that there is a nearly linear relationship between the strain and the voltage across the films that are subjected to both compressive and tensile stress. Futhermore, Kang et al. [10] dispersed the SWCNTs in DMF solvent and sonicated for 20 h and after that, the solution was poured into filter paper. Moreover, he proposed an electrical model of the CNT strain sensor by using electrochemical impedance spectroscopy to simulate the dynamic response of sensor. The resistance was found to change almost linearly under the application of a micro strain. Li et al. [111] used as grown SWCNTs and monitored the linear relation between the shifts in the G bands and the tensile strain by raman spectroscopy. The linear relationship between the shift and tensile strain confirms that SWCNTs are strained and the application of the strain changes the electrical properties.

The restrictions in the SWCNT buckypapers as strain sensors such as the influence of chirality, purity and the electrical properties rise the demands through the utilization of MWCNTs. In comparison with SWCNTs, MWCNT overcome the limitations in terms of cost effectiveness and purity [112]. Numerous studies have been carried out aiming to reveal the capability of using MWCNT thin films as strain sensor. Li et al. [113] used MWCNTs prepared by the solution / filtration method and the films were bonded directly on the specimens. An unaxial load/unload tensile test has been used twice to determine the repeatability and characterization of the strain sensor behavior of the MWCNT thin film as it is illustrated in Fig. 6.8. The obtained results indicate that the strain sensing is repeatable and the sensor is suitable for structural health monitoring (SHM) and vibration control applications. Vemuru et al. [114] used also MWCNTs for strain sensing. The MWCNTs were suspended using Nanosperse AQ surfactant and then sonicated for 30 min. The suspension was then filtered using porous filters under pressure. A linear response of voltage as function of strain was measured using a four point probe. Additionally, it was observed that the MWCNT films show high recovery conditions upon unloading.
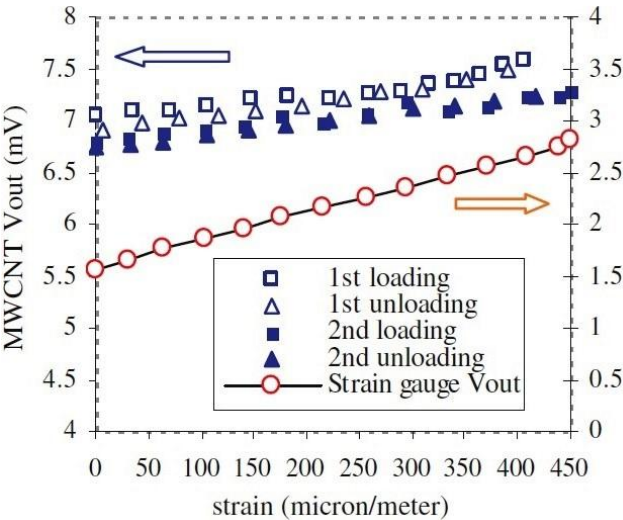
FIGURE 6.8
MWCNT voltage output in comparison with foil strain gage voltage output [114]

Dinh et al. [115] investigated the piezoresistivity of the MWCNTs films dispersed in SDS surfactant on the PET substrate by the inkjet printing technique. The films were undergone to the force testing machine and the resistance changes monitored with a Whitestone bridge circuit coupled with a lock-in amplifier. The results showed a linear response (Fig. 6.9) after the second cycle and a low hysteresis which means that the sensor is appropriate as strain sensor.
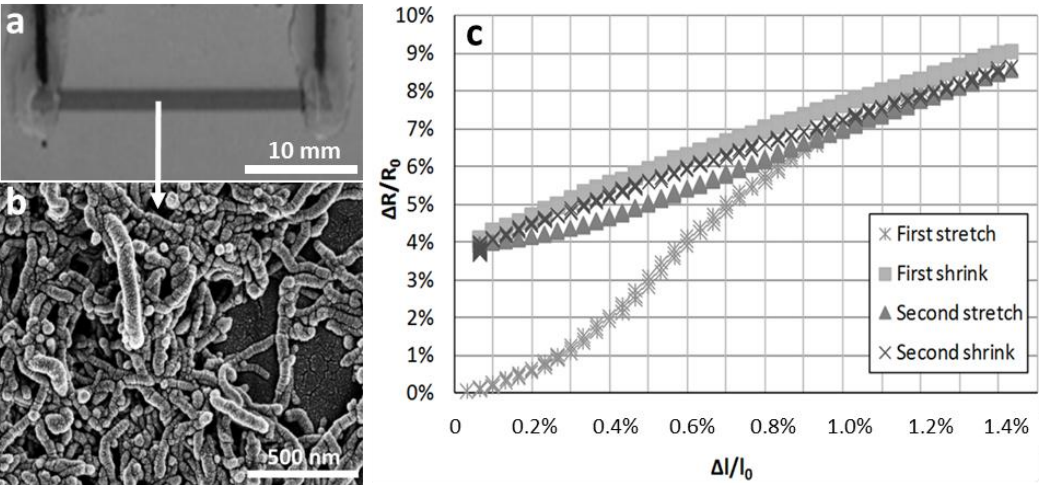

FIGURE 6.9
MWCNT films deposited by inkjet printing. a) Optical microscopy image of a CNT film with a size of 2 mm × 30 mm. b) Corresponding SEM image of the CNT film. (**c**) Change of resistance *vs.* strain at first and second cycle in tensile test, redrawn from [115]

Current investigations concerning the improvements in CNT based strain sensors have succeeded a great achievement owing to their outstanding properties in comparison with traditional strain sensors. Besides that, there are some certain parameters that have to be investigated in order to obtain a good sensor for practical applications. It has been investigated that processing parameters such as sonication time, type of surfactant and temperature has an observable influence on sensor behavior. Wang et al. [116] investigated the strain-induces resistance changes in iodine-doped and undoped CNTs and it was found that under 500 microstrain at room temperature the gauge factors were about 125 and 65 for I-doped and undoped CNT films respectively. The main factors that influenced the piezoresistivity of the CNT film are ascribed to strain-induced changes in the band gap and the change of intertube contact resistance. Dinh et al. [117] compared the effect of different surfactants such as SDS, deoxycholic acid (DOC) and a polymer composite polyethylene oxide (PEO) on the piezoresistive properties of MWCNTs. The films were fabricated by drop casting on the specimens and they were undergone to the extensometer and simultaneously the change in resistance was recorded. All films showed a nearly linear response under applied strain with the following gauge factors 4, 7.5 and 12.5 for SDS, DOC and PEO, respectively. Bu et al. [72] analyzed the effect of sonication time and surfactant concentration on the resistivity of both SWCNT and MWCNTs films. It has been demonstrated that the uniformity and the reproducibility of the CNT films were highly enhanced by the sonication time. In Fig. 6.10, the sensing characteristics of SWCNTs and MWCNTs under strain are shown. With a strain up to 0.1 %, MWCNTs show better sensitivity than SWCNT. Furthermore, for the MWCNTs two regions were observed due to variation of contact and intrinsic resistance of the films under strain. In other words, in the low strain region, the sensitivity is attributed mainly to the change of the contact resistance between the tubes. However, at high strain besides the alteration of contact resistance, changes in the bandgap of individual tubes occur and these alterations result in higher strain sensitivity [118-120].
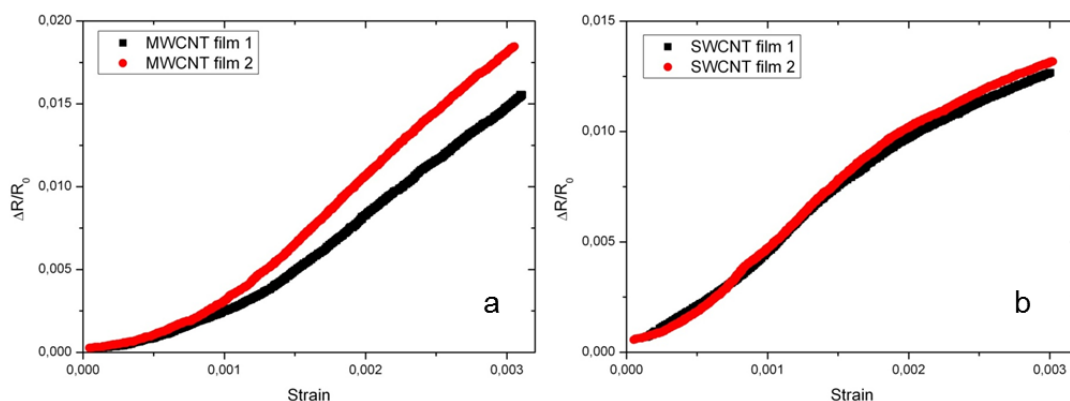

FIGURE 6.10
The relative change of film resistance with strain for CNT films with 0.5 wt.% SDS and 15 min sonication time a) MWCNTs. b) SWCNT, [72]

Vemuru et al. [114] investigated the temperature effect by heating the specimen and recorded the resistance change simultaneously. It was observed that the resistance of MWCNT film decreases with temperature. The resistance of the film changed about 0.0217 Ω at a temperature difference of 13.9 ˚C. Hone et al. [121] observed a resistance change for magnetically aligned SWCNT samples before and after annealing. It was found that the SWCNTs aligned in both parallel and

perpendicular directions, exhibits similar behaviors at temperatures up to 300 K. Barberio et al. [122] investigated the electrical resistivity of MWCNT samples in the temperature range from 300 K to 1900 K. It was reported that MWCNTs show a monotonous decrease of resistivity with increasing temperature.

CNT/Polymer Composite Strain Sensor

CNT/polymer composites have improved mechanical properties than pure polymers. Commonly CNTs embedded in a polymer have higher sensitivity than CNT films without polymer. Dinh et al. reported about a sensitivity of 12.5 by using DOC as tenside [115]. On the other hand a maximum sensitivity of 22.4 was reported in epoxy [93]. In general, CNT/polymer based strain sensors can be applied to several measurement ranges due to consideration of different kinds of polymers. Depending on the polymer also strains of lower than 0.25% typically applied to metal DMS can be detected. However, the unbundling process of CNTs in a polymer is a challenging task. Additionally, the attachment between CNT and polymer and between composite and the measurement object need further development.

Different possibilities were investigated for dispersions of CNT/polymer composite strain sensors, such as sonication, stirring and calendering. For thermoplastic polymers melt processing, stirring and hot pressing are preferred [36]. For elastomers and thermosets in-situ polymerization is often used which leads to a good cohesion between the CNTs and polymer. For deposition, very often mould casting and screen printing is favoured. In some investigations LBL technology is used [123-125]. For the same CNT concentration, CNT/polymer composites in elastomer matrix have a higher conductivity than thermoplastic and thermoset based composites. For instance, Mechrez et al. [126] reported that the conductivity could reach up to 1000 S/m for polyacrylate with 10 wt% CNTs. Chen et al. [127] found a conductivity of 280 S/m for randomly distributed MWCNTs (1.3 wt%) in PDMS . In contrast, in thermoset and thermoplastic matrices the conductivity ranges between 0.1 S/m to 50 S/m with the same CNT concentration [127- 130].

The sensitivity of nanocomposite can be predicted by measuring the viscosity of the dispersion. This fact can be helpful for the development of strain gauge with high sensitivity. In order to achieve a high sensitivity, a high conductivity in the saturation area is not useful (see Fig. 6.4). Based on the study of Ramasubramaniam et al. [125] for SWCNT/PPE composites the highest sensitivity can be achieved in the conductivity range from 0.1 S/m to 10 S/m. Sensitivity data obtained from SWCNT/polymer and MWCNT/polymer composites are summarized in table 1. For an easy comparison of the data it was assumed that 1 vol% SWCNTs is equivalent to 1 wt% and 1 vol% MWCNTs is equivalent to 2 wt% [36].

Generally, a lower concentration leads to lower conductivity and therefore a higher sensitivity. The best gauge factor in the studied literature (see table 1) reported by Yin et al. [123] is 22.4. For epoxy as polymer, they used in-situ polymerization and applied planetary mixing. It was found that alignment of CNTs leads to improved linearity of the strain dependent resistance change. Whereas, randomly distributed CNTs have two ranges with different sensitivity in their strain/resistance characteristic [123,131].

Unlike metallic strain gauges, which have a low resistance, the high resistance of CNT/polymer composite is a challenge for the signal processing. Due to the presence of tunneling effects within the composite, the conductivity of the nanocomposite strongly depends on the temperature. Furthermore the temperature noise increases with increasing resistance. Therefore, comprehensive investigations have to be made between temperature cross-sensitivity, temperature noise and the sensitivity.

TABLE 6.1
Experimental parameters for CNT/polymer film and corresponding strain sensor parameters. Acronyms: PMMA (polymethyl methacrylate), PVA (polyvinyl acetate), PSS (poly(sodium 4-styrene-sulfonate)), PSF (Polysulfon), PEO (polyethylene oxide)

Filler (diameter; length)	Polymer	Fabrication method	Conductivity [S/m]	Gauge Factor (amount of CNT)	Ref
SWCNT	PMMA	buckypaper filled with PMMA	-----	5.3 (0.5 wt. %)-1 (10 wt. %)	[10]
SWCNT	PVA, PSS	solution mixing; Layer by layer, thin film	-----	0.208	[128]
SWCNT	PVA, PSS	solution mixing; Layer by layer, thin film	-----	1.805	[129]
MWCNT (60 − 100 nm; 0.5 − 500 µm)	PMMA	bulk mixing then melt processing (film: 0.127mm)	-----	15.32 (1 wt. %) 4.59 (3 wt. %) 4.26 (5 wt. %) 3.27 (6 wt. %) 1.9 (8 wt. %) 1.44 (10 wt. %)	[130]
MWCNT (10 − 20 nm; Several µm)	epoxy	in-situ polymerization (three roll mill); mould casting	1×10^{-4}	0.75 (0.1 wt. %)	[132]
MWCNT (10 − 20 nm; Several µm)	epoxy	in-situ polymerization (three roll); mould casting	2×10^{-4} 1.32×10^{-2}	4.5 (0.1 wt. %) 3.5 (0.3 wt. %)	[133]
MWCNT (10 nm; 5 − 15 µm) small and curved shapes	epoxy	in-situ polymerization (planetary mixer); mould casting	7.07×10^{-4} (5 wt. %) 1.92×10^{-3} (7 wt. %) 5.33×10^{-3} (10 wt. %) 4.49×10^{-2} (15 wt. %)	4.9 (5 wt. %) 4.5 (7 wt. %) 5.8 (10 wt. %) 4.4 (15 wt. %)	[123]
MWCNT (40 − 90 nm; 5 − 10 µm) straight shapes	epoxy	in-situ polymerization (planetary mixer); mould casting	10.4 (5 wt. %) 65.8 (7 wt. %) 95.2 (10 wt. %) 125.1 (15 wt. %)	22.4 (1 wt. %) 7.6 (4 wt. %) 6.2 (5 wt. %) 4.8 (7 wt. %) 3.2 (10 wt. %)	

MWCNT (40 nm; 4 - 6 μm)	epoxy	in-situ polymerization (planetary mixer); mould casting	0.02 (1 wt. %) 1 (2 wt. %) 10 (5 wt. %)	22.4 (1 wt. %) 12 (2 wt. %) 6 (5 wt. %)	[31]
MWCNT (40 - 90 nm; 10 - 30 μm)	epoxy	in-situ polymerization (planetary mixer)	3.3×10^{-2} (1 wt. %) 1.13 (2 wt. %) 10.4 (5 wt. %)	22.4 (1 wt. %) 11.6 (2 wt. %) 6.2 (5 wt. %)	[134]
MWCNT (4 – 13 nm; 1 – 4 μm)	PSF	solution mixing then mould casting in AC electrical field (aligned)	-----	2.68 (0.5 wt. %) 1.82 (0.75 wt. %)	[45]
MWCNT (4 – 13 nm; 1 – 4 μm)	PSF	solution mixing then mould casting; (randomly distributed)	-----	0.73 (0.75 wt. %, < 0.5% strain) 1.57 (0.75 wt. %, >0.5% strain)	
MWCNT	PEO	solution mixing; mould casting	-----	3.7 (1.12 wt. %, < 0.85% strain) _____1 .6 (2.9 wt. %, < 2% strain) 50 (2.9 wt. %, > 2% strain)	[131]

In order to explain the experimental results theoretical investigations have been performed. Thereby effects like destruction and formation of conductive paths which take place when a strain is applied were considered. However, the dominant effect in sensitivity is not predictable yet. Especially the increasing resistance in elastomers by extension and compression shows a discrepancy with the simulation results [62]. At low CNT concentrations in the nanocomposite large conductivity fluctuations may occur due to the strong influence of destruction and formation of conductive paths [130]. This behavior has been experimentally and theoretically confirmed by Hu et al. [31].

CNT Yarns as Strain Sensor

CNT buckypapers are not ideal for strain sensors that require multi-functionality and repeatability as well as their easy deformation under the strain. Therefore, CNT yarns have been proposed for strain sensor applications to overcome the aforementioned limitations. Zhao et al. [13] developed an embeddable CNT yarn strain sensor for monitoring the cracks in composite structures by twisting individual CNT arrays. It was pointed out that the pure CNT yarn can be utilized as a strain sensor which shows no hysteresis, high repeatability at temperatures ranging from 77 K to 373 K and high resistance-strain behavior. The CNT yarn sensor has been tested under two different tensions namely longitudinal and transverse tension. It has been found that the resistance of the CNT yarn increases linearly under longitudinal tension, while a nonlinear response with very low resistance change is observed for transverse tension. Shang et al. [136] adopted a simple structural

modification for fabrication of elastic and highly conductive CNT yarns (R on the order of 10 Ω) by using a number of helical loops for strain sensor application. It has been revealed that such elastic yarns can be continuously stretched up to 25 % for 1000 cycles without any deformations and with a linear change of electrical resistance under the strain. The relative resistance change is very reversible over 1000 cycles and reproducible. Under the 25 % elongation of the spring the relative change is found to be 3.2%.

Li et al. [137] have shown the possibility of overtwisting the helical nanotube yarns into a highly entangled structure for 600 cycles and then resolving it in order to investigate the repeatability and potential of overtwisted SWCNT strain sensors for high strain ranges up to 500 % (Fig. 6.11).
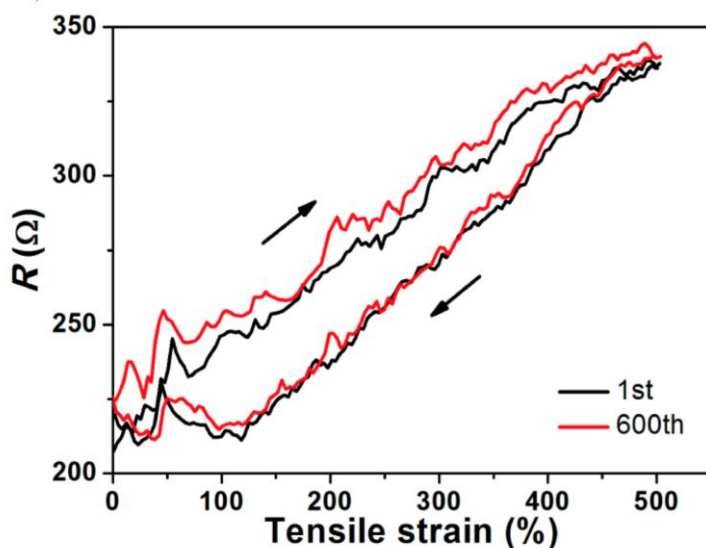

FIGURE 6.11
Electrical resistance change under strain for the first cycle and after 600 cycles [137]

Li et al. [137] also showed that, CNT overtwisted yarns show roughly linear response. The stable relative resistance change (after 100 cycles) shows that the sensor is highly reproducible and stable for strain sensor applications. Moreover, Kahng et al. [138] have demonstrated the multi-functionality of the MWCNT yarns placed on both sides of a stainless steel test beam that measuring both strain and temperature simultaneously. In order to compare the resistance profile of MWCNT yarns with conventional strain gauges, two Wheatstone bridge configurations have been built up and the strain and temperature measurements are carried out by reading the data from bridge outputs. The results showed that the stress-strain responses are repeatable for 50 cycles. However, the strain response was limited to 3 % strain and cyclic strain-stress responses exhibited a degree of hysteresis that need to be further investigated.

Pressure Sensor based on CNTs

In this chapter, the influence of various processing parameters such as CNT type, CNT orientation, fabrication technique, polymer type, temperature and substrate flexibility have been introduced. These factors are significant and they need to be optimized for pressor sensors fabrication.

Furthermore, a systematic investigation with respect to sensitivity, hysteresis and measurement range are taken into account to address the different fields of applications.

Influence of processing parameters on pressure sensor performance

As an alternative to the pressure sensor based polysilicon, Fung et al. [139] proposed a pressure sensor based on MWCNTs deposited on flexible polymethylmethacrylat (PMMA) substrates using dielectrophoresis (DEP). The proposed pressure sensor based on CNTs was of low-cost and had positive gauge factor of 5 to 10 times higher than conventional polysilicon sensors. Qian et al. [140] used MWCNTs arrays as the field emitters to develop a field emission pressure sensor. The hot filament chemical vapor deposition (HF-CVD) was used to grow the MWCNT on single crystalline n-Si wafer. Latter one was utilized as the cathode. An elastic membrane fabricated by wet etching process was used for the anode. The pressure sensitivity was measured to be about 0.16–0.78 nA/Pa (101–550 kPa), with very low hysteresis effect. However, this sensitivity could be controlled by changing the distance between the anode and the cathode and adjusting the thickness of the elastic membrane. Slightly increase in the emission current under the same pressure for the unloading cycle was observed, which could be induced by the deformation recovery lagging effect.
Gau et al. [141] fabricated a micropolymer pressure sensor using Polyimide (PI) reinforced with MWCNTs nanocomposites thin films nanocomposite covered with SU-8 membrane. The sensor sensitivity showed high linearity for low MWCNTs concentration, as it is shown in Figure 6.12. The sensor resolution was found to be 5.08 ΩkPa^{-1} (35 Ω/psia), which is almost twice than the polysilicon sensor reported in [142]. This micropolymer pressure sensor has also rapid response, and is thermally stable. Beside this fact, it was found that the gauge factors could be improved by using thinner diaphragms and lower CNTs concentration.
In order to improve the sensitivity and sensing linearity, Wang et al. [143] dispersed two different kinds of MWCNTs (non-functionalized and MWCNTs with carboxyl functional group (−COOH) as fillers in silicone rubber. He found that that functionalized MWCNTs samples had four times higher resistance and sensitivity than non-functionalized MWCNTs. This increase in the sensitivity is due to formation of 3-D CNT networks, which is caused by the improvement in the homogeneous distribution and alignment of the MWCNTs within the polymer matrixes [143].
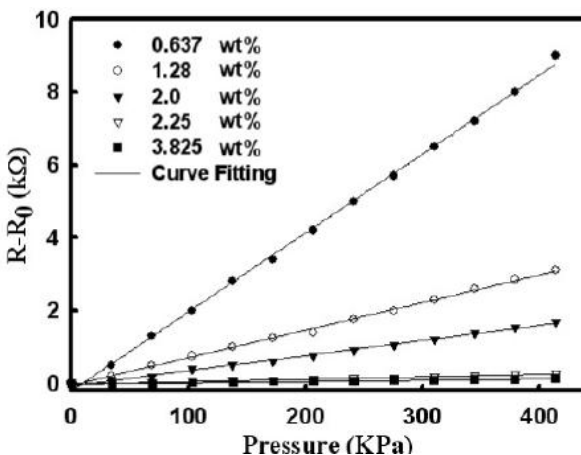

FIGURE 6.12
The resistivity variation with air pressure for nanocomposites at different MWNT contents [141]

Gau et al. [141] also studied also the effect of temperature on the composites, which showed a semiconducting behavior in the temperature range of 20 to 100°C. For this reason, the temperature coefficient could be determined and subtracted later from the measurements.

Mohiuddin et al. [144] studied the pressure-dependent electrical resistance of MWCNT- polyether ether ketone (PEEK) composites under different temperature environments for different CNT content. Increasing the pressure reduced the electrical resistance. It was observed that the effect of the pressure is more visible at room temperature then at 140°C (below the glass transition temperature of PEEK 146°C). At room temperature, the pressure sensitivity was higher in the lower pressure range (from 0 to 20 MPa) and for pressure ranges more than 20 MPa, almost no pressure effect was measured.

Effect of Alignment

Rather than using randomly distributed CNTs, Yilmazoglu et al. [145] designed a thin and flexible pressure sensor based on vertically aligned MWCNT arrays sandwiched between two carbon layers. Gold contacts pads were sputtered on the top side of the sensor. The bulk resistance of the sensor ranged between 30 Ω and >10 kΩ, and was found to depend on many parameters such as, contact size, growth condition, tube diameter and wall thickness. These parameters affected also the sensitivity of the sensor, since smaller contact pads lead to higher sensitivity. For 5μm displacement, a change of 35% of resistance and high reproducibility were observed.

On other hand, Taak et al. [146] fabricated field emission pressure sensors based on vertically grown CNTs inside an array of micromachined holes by plasma-enhanced chemical vapor deposition (PECVD) and then covered them with the bulk Si to ensure the electrical isolation and different operation modes of the anode. Indeed, the prepared sensor achieved a wide dynamic range and a high sensitivity by allowing anode/cathode proximity and preventing electrical short circuit. Due to the deflection of the membrane a non uniform spacing between anode/cathode can be generated over the sample area that lead to non-uniform field emission behavior of CNTs. Two regimes in the slope of emission current; a linear regime at the low pressure and a nearly saturated regime for full-range pressures were observed.

Recently, Haniff et al. [147] used horizontally orientated CNTs onto flexible polyimide substrate to fabricate highly sensitive pressure sensors. Under an in-plane pressure force ranging from 0 to 50 kPa, a high sensitivity at small changes of pressure was demonstrated. In addition, to the high performance region reaching about 1.68 % / kPa, this result was achieved by the enhancement of the contact area and the tunneling distance per nanotube upon stretching caused by the weak van der Waals forces between the nanotubes and the large portion of isolated nanotubes, as it is depicted in Figure 6.13. This sensitivity is claimed to be the highest up to date and was approximately 27, 17, 2, and 3.5 times higher than those reported in [148, 149-151].
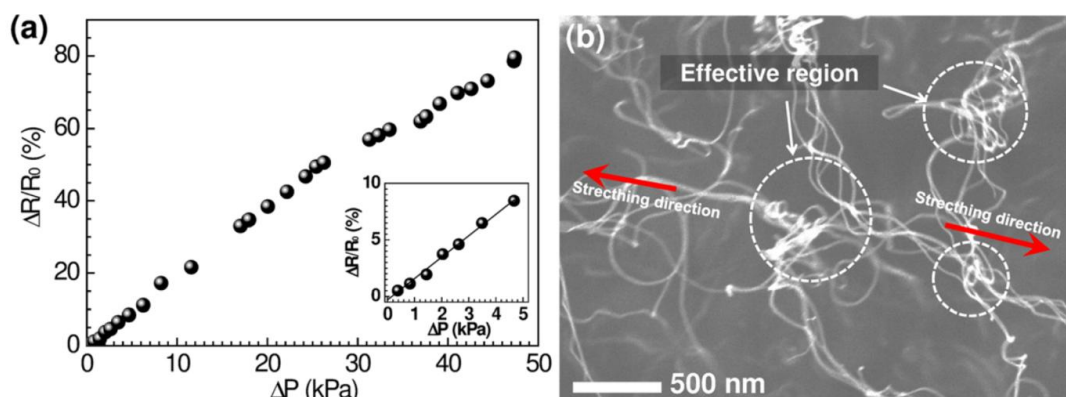
FIGURE 6.13
Performance of the horizontally oriented MWCNTs as pressure sensor. a) Relative change in resistance as function of the applied pressure. b) Structure of the nanotubes during stretching [147]

So et al. [152] used vertically aligned MWCNTs (VACNTs) embedded in polydimethylsiloxane (PDMS) matrix and connected to a SWCNT-Field effect transistor (FET) for fabrication of pressure sensors. Upon repeated compression, this sensor showed high flexibility owing to the high elasticity of the PDMS and VACNTs. A negative gauge factor was observed, where a decrease in the resistance from 335 Ω to 275 Ω under a pressure 275 kPa was observed. On the other hand, the pressure force induces denser current paths and thus enhances the CNT/metal contacts. This will also lead to an increase in the conductance of the CNTs caused by the VACNTs. However, by controlling the length and hardness of the VACNTs and the PDMS, respectively, the pressure sensitivity could be adjusted.

Sepúlveda et al. [153] developed a capacitive pressure sensor composed of three thin layers, the upper and the bottom layer were used as electrodes consisting of 1% of aligned CNTs embedded in PDMS. A tension test was applied in both axial and transverse directions using an Instron 4505 universal testing system. Generally, this CNT/PDMS nanocomposite showed non-isotropic elastic behavior. The Young's modulus was increased for both transverse direction and the axial direction to 1.7 MPa and 8 MPa respectively. By changing the pressure from 100 kPa to 30 kPa, the change in capacitance was determined by placing the sensor inside a controlled pressure chamber. Bsoul et al. [148] designed pressure sensors using Si-micromachining techniques. The pressure sensor formed with vertically aligned CNTs (VACNTs) forest was grown on Si substrate and covered with Parylene-C membrane. Upon positive and negative gauge pressures, the sensor showed sensitivities comparable in magnitude for both with the average values of -986 and +816 ppm/kPa. The decrease in the resistance for the case of positive pressure was explained by the narrowing of the separation around the two border regions between the substrate and the membrane and the opposite for the case of negative pressure.

Future Development of CNT pressure and strain sensors

Recently, a lot of progress has been achieved in increasing the strain sensitivity and understanding the working mechanism, which is of high importance for practical applications. However, up to now

only a few studies have been reported about the stability and reproducibility of CNT strain sensors. There are some examples related to structural health monitoring [11,124,154,155].

For instance, Yamada et al. [11] used SWCNT on PDMS to measure human motion by assembling the sensors on bandages or on clothes. Furthermore, these sensors were used for real time monitoring of biological functions of the human body such as breathing and phonation. Loh et al. [124] used LBL technique to fabricate CNT-polymer composite thin films for sensing skin for impact monitoring and crack detection. When dynamic load with uniaxial tension and compression were applied on cementitious bars, micro cracks were monitored. Shindo et al. reported the use of CNT/polymer composites for crack detection and propagation [154]. The crack sensing was measured at room temperature and at 196 °C, and they found a strong relationship between the resistance and the crack length. Inam et al. in [155] proposed a novel method for the SHM based on alumina nanocomposites filled with different carbon nanoparticles (graphene nanoplatelets (GNP), CNTs and carbon black nanoparticles (CB)). Among them CNTs showed the best sensing properties with 86% decrease of the elecrtrical conductivities. The previously mentioned results show a great potential of CNTs for SHM application.

Another interesting option for CNT based films are wireless strain sensors. Conventional strain sensors can only measure the strains directly on the structural surface; therefore cables need to be applied, and this makes it difficult for some applications, e.g. vibrational applications. Hence, there is a need to develop wireless strain sensors which can work in harsh environment and detect the strain wirelessly. For this purpose CNT films can be easily patterned. Loh et al. [156] used SWCNT/PVA LBL deposition to pattern a coil antenna onto PET flexible substrate and measured the impedance response of the films under strain wirelessly. The schematic illustration is depicted in Fig. 6.14.
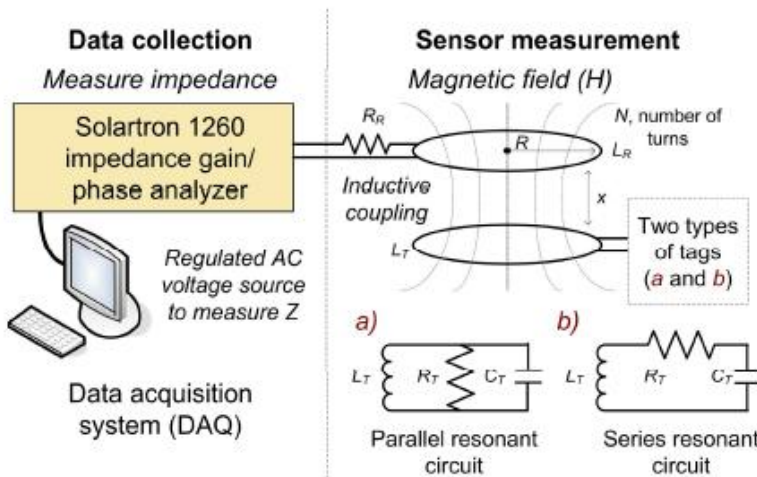

FIGURE 6.14
A schematic illustration of wireless strain sensor based RFID Technique adapted from [156]

The fabricated coil based SWCNT/PVA LBL form an RC-circuit type thin film; by subjecting the coil specimens to tensile-compressive cycle loading, an equivalent parallel-RC circuit models is proposed to fit the experimental data and characterize the electrical-mechanical behavior of the

thin film. Due to changes of its R and/ or C values, the strain can be detected wirelessly through the shifts in the characteristic frequency of the coil and/ or changes in its bandwidth (Fig. 6.15).
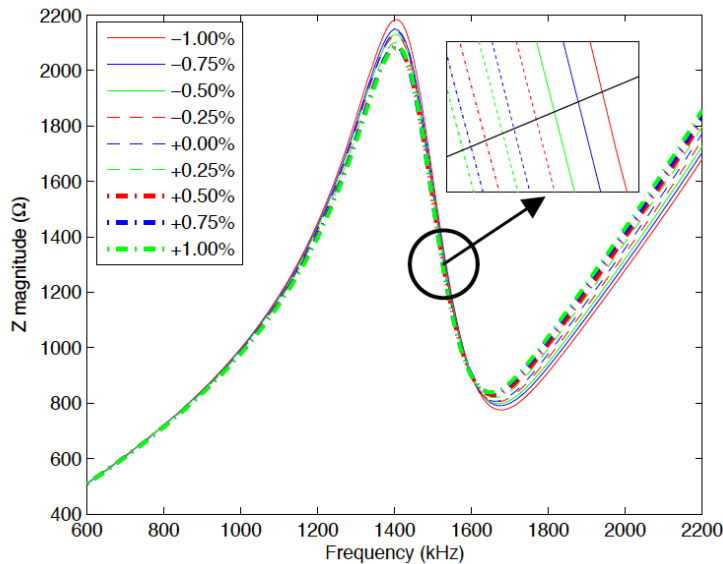

FIGURE 6.15
Experimental RFID reader response of SWCNT on PET capacitive strain sensor [156]

Benchirouf et al. [157] used inkjet printing instead of LBL deposition to pattern the MWCNTs dispersed in SDS and patterned them as planar coils onto PET-flexible substrates, as it is shown in Fig. 6.16 (a). Coils with different number of windings, and number of deposited layers were investigated. The self-resonance frequency was in the range of 11-13 MHz. The measurement setup is shown in Fig. 6.16 (b).
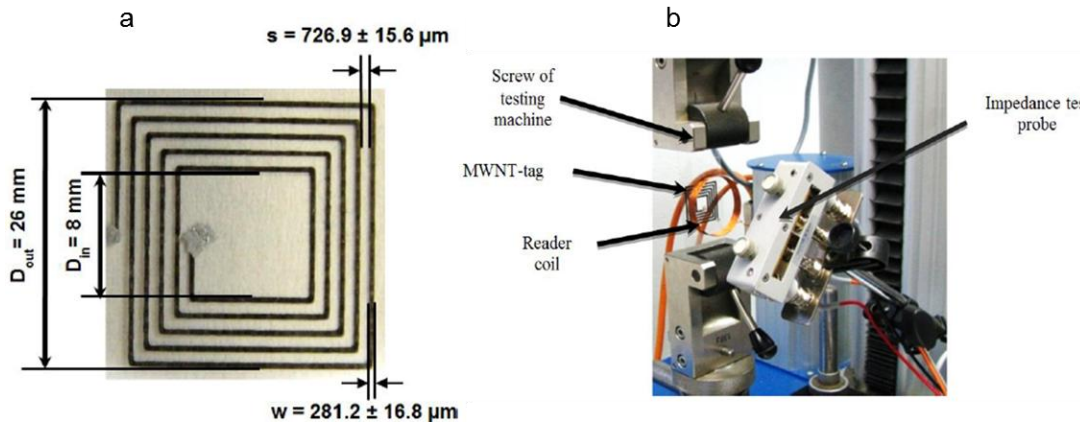

FIGURE 6.16
a) Printed coil with 5 windings and the coil parameters - outer diameter (D_{out}), inner diameter (D_{in}), line width (w) and line distance (s); b) Measurement setup for the sensor coupling [157]

Due to the very small changes of the coil capacitance, no shift in the resonance frequency was detected. Instead of that, changes in the bandwidth and amplitude were clearly identified (Fig. 6.17). Linear trends of these shifts as function of force were observed for both loading and unloading cycles, with almost no hysteresis effect. Tang et al. [158] used vacuum filtration and a transfer process to fabricate flexible and uniform MWCT embedded in polydimethylsiloxane (PDMS) sheets for wireless strain sensing. Simulations complementarily perfomed to the experimental part showed that the conductivity of the path dramatically affects the sensing properties by altering the gain and the return loss. A minimum conductivity of 105 S/m was necessary to have an acceptable gain and return loss. A displacement of 1500 µm was founf to give a shift of 6.5 % in the resonance frequency. Tata et al. [159] fabricated amorphous carbon strain sensor on a flexible substrates and integrated them in a wireless module for human motion detection. The amorphous carbon was sputter-deposited on a 125 µm thick polyimide film and the strain gauges were tailored using laser micromachining. Finally, the packaged sensor was encapsulated into elastic PDMS polymer. The human body motion induced deformations in the antenna structure. A linear change of the resistance over the applied strain was monitored.
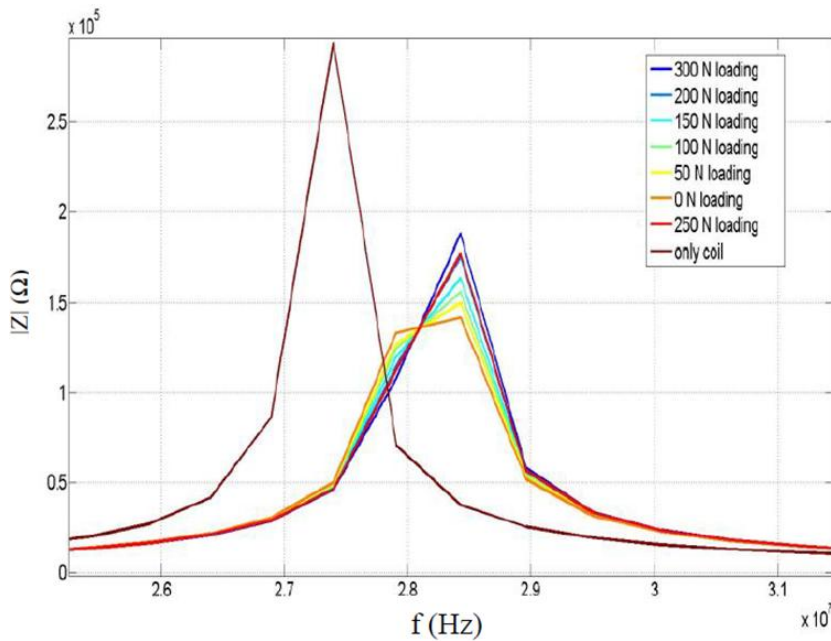

FIGURE 6.17
Coupling response of a coil sensor with 5 windings under load [157]

Conclusions and Outlook

In this contribution, CNT based films for high performance pressure and strain sensors on flexible substrates have been reviewed. Besides outstanding physical properties of CNTs, limitations of CNTs such as the tendency to aggregation, hydrophobic and poor solubility in aqueous and organic solvent influences on the properties of CNT based nanocomposites. In order to acquire an efficient preparation of CNT dispersions and CNT/polymer composites we focused firstly on the effects of various surfactant types and deposition techniques on CNTs physical properties. It was found that the efficiency of CNT dispersion strongly depends on properties of solvents, CNT and polymer types. For instance, using SDBS as surfactant leads to higher dispersion in comparison with SDS and triton X-100 surfactant.

The parameters that influence the resistance properties of CNT films can be described based on the two dimensional stick percolation theory which helps to understand the electrical conduction mechanism of CNT based nanocomposite matrix. The percolation threshold and conductivity depend strongly on the polymer type, fabrication parameters, aspect ratio of CNTs, disentanglement of CNT agglomerates, uniform spatial distribution of individual CNTs and degree of alignment. Furthermore, a strong influence of the fabrication parameters on the CNT films strain sensor performance and reproducibility were shown.

Experimentally, it was found that the strain sensor sensitivity is greatest at the percolation threshold of CNT/polymer based nanocomposites that depends on many factors, e.g. aspect ratio, CNT type, shell quality, dispersion degree and functionalization of the CNTs which in turn defines the sensitivity of CNT/polymer composite strain sensors. For this purpose, an overview has been given for determining the effects of different type of filler, polymer and fabrication process on the strain sensitivity.

By comparing the sensitivity of SWCNT and MWCNT, it can be concluded that SWCNTs add no advantage to the CNT film strain sensors although they show intrinsic semiconducting and metallic behavior in the CNT network. From experimental and theoretical findings, it is difficult to predict which effect is dominating when strain is applied and conductivity fluctuation occurs at low CNT concentration due to destruction and formation of conducting paths.

Consequently, controlling and understanding the influence of the CNT film parameters on the sensor properties are crucial for strain sensor applications. Although there are numerous studies that have been conducted, the CNT based pressure and strain sensors have still to be more investigated in parallel to the development of nanotechnology until they will achieve the desired properties for commercial applications.

References

1. Kulha, P.; Boura, A.; Husak, M. Design and fabrication of piezoresistive strain-gauges for harsh environment applications. In Proceedings of the International Conference on Renewable Energies and Power Quality (ICREPQ), Granada, Spain, 23–25 March **2010**, *10*, 510.
2. Tanner, J.L.; Mousadakos, D.; Giannakopoulos, K.; Skotadis, E.; Tsoukalas, D. High strain sensitivity controlled by the surface density of platinum nanoparticles. *Nanotechnology* **2012**, *23*, 285501.

3. Sangeetha, N.M.; Decorde, N.; Viallet, B.; Viau, G.; Ressier, L. Nanoparticle-based strain gauges fabricated by convective self assembly: Strain sensitivity and hysteresis with respect to nanoparticle sizes. *J. Phys. Chem. C* **2013**, *117*, 1935–1940.

4. Tanner, J.L.; Mousadakos, D.; Broutas, P.; Chatzandroulis, S.; Raptis, Y.S.; Tsoukalas, D. Nanoparticle strain sensor. *Proc. Eng.* **2011**, *25*, 635–638.

5. Zhang, W.; Zhu, R.; Nyugen, V.; Yang, R. Highly sensitive and flexible strain sensors based on vertical zinc oxide nanowire arrays. *Sens. Actuators A Phys.* **2014**, *205*, 164–169.

6. Wu, J.M.; Chen, C.Y.; Zhang, Y.; Chen, K.H.; Yang, Y.; Hu, Y.; He, J.H. and Wang, Z.L. Ultrahigh sensitive piezotronic strain sensors based on a $ZnSnO_3$ nanowire/microwire. *ACS Nano* **2012**, *6*, 4369–4374.

7. Wang, B.; Lee, B.K.; Kwak, M.J.; Lee, D.W. Graphene/polydimethylsiloxane nanocomposite strain sensor. *Rev. Sci. Instrum.* **2013**, *84*, 105005.

8. Tian, H.; Shu, Y.; Cui, Y.L.; Mi, W.T.; Yang, Y.; Xie, D.; Ren, T.L. Scalable fabrication of high-performance and flexible graphene strain sensors. *Nanoscale* **2013**, *6*, 699–705.

9. Kuang, J.; Liu, L.; Gao, Y.; Zhou, D.; Chen, Z.; Han, B.; Zhang, Z. A hierarchically structured graphene foam and its potential as a large-scale strain-gauge sensor. *Nanoscale* **2013**, *5*, 12171–12177.

10. Kang, I.; Schulz, M.J.; Kim, J.H.; Shanov, V.; Shi, D. A carbon nanotube strain sensor for structural health monitoring. *Smart Mater. Struct.* **2006**, *15*, 737.

11. Yamada, T.; Hayamizu, Y.; Yamamoto, Y.; Yomogida, Y.; Izadi-Najafabadi, A.; Futaba, D.N.; Hata, K. A stretchable carbon nanotube strain sensor for human-motion detection. *Nat. Nanotechnol.* **2011**, *6*, 296–301.

12. Zhang, W.; Suhr, J.; Koratkar, N. Carbon nanotube/polycarbonate composites as multifunctional strain sensors. *J. Nanosci. Nanotechnol.* **2006**, *6*, 960–964.

13. Müller, C.; Leonhardt, A.; Kutz, M.C.; Reuther, H. Growth aspects of iron-filled carbon nanotubes obtained by catalytic chemical vapor deposition of ferrocene. *J. Phys. Chem. C* **2009**, *113*, 2736–2740.

14. Stampfer, C.; Helbling, T.; Obergfell, D.; Schöberle, B.; Tripp, M.K.; Jungen, A.; Hierold, C. Fabrication of single-walled carbon-nanotube-based pressure sensors. *Nano Lett.* **2006**, *6*, 233–237.

15. Iijima, S. Helical microtubules of graphitic carbon. *Nature* **1991**, *354*, 56–58.

16. Choudhary, V. and Gupta, A. Polymer/Carbon Nanotube Nanocomposites, Carbon Nanotubes - Polymer Nanocomposites; Intech: 2011.

17. Pauliukaite, R.; Murnaghan, K.D.; Doherty, A.P.; Brett, C. A strategy for immobilisation of carbon nanotubes homogenised in room temperature ionic liquids on carbon electrodes. *J. Electroanal. Chem.* **2009**, *633*, 106–112.

18. Prasek, J.; Drbohlavova, J.; Chomoucka, J.; Hubalek, J.; Jasek, O.; Adam, V.; Kizek, R. Methods for carbon nanotubes synthesis-review. *J. Mater. Chem.* **2011**, *21*, 15872–15884.

19. Frank, S.; Poncharal, P.; Wang, Z.L.; de Heer, W.A. Carbon nanotube quantum resistors. *Science* **1998**, *280*, 1744–1746.

20. Bachtold, A.; Strunk, C.; Salvetat, J.P.; Bonard, J.M.; Forró, L.; Nussbaumer, T.; Schönenberger, C. Aharonov–Bohm oscillations in carbon nanotubes. *Nature* **1999**, *397*, 673–675.

21. Dresselhaus, M.S.; Dresselhaus, G.; Eklund, P.C. *Science of Fullerenes and Carbon Nanotubes: Their Properties and Applications*; Academic Press: New York, United States, 1996.

22. Yu, M.F.; Lourie, O.; Dyer, M.J.; Moloni, K.; Kelly, T.F.; Ruoff, R.S. Strength and breaking mechanism of multiwalled carbon nanotubes under tensile load. *Science* **2000**, *287*, 637–640.

23. Ruoff, R.S.; Tersoff, J.; Lorents, D.C.; Subramoney, S.; Chan, B. Radial deformation of carbon nanotubes by van der Waals forces. *Nature* **1993**, *364*, 514–516.

24. Yu, M.F.; Files, B.S.; Arepalli, S.; Ruoff, R.S. Tensile loading of ropes of single wall carbon nanotubes and their mechanical properties. *Phys. Rev. Lett.* **2000**, *84*, 5552–5555.

25. Yang, L.; Anantram, M.P.; Han, J.; Lu, J.P. Electro-mechanical properties of carbon nanotubes. *Phys. Rev. B* **1998**, *60*, 13874.

26. Li, C.; Chou, T.W. Strain and pressure sensing using single-walled carbon nanotubes. *Nanotechnology* **2004**, *15*, 1493–1496.

27. Zettl, A.; Cumings, J. Electromechanical properties of multiwall carbon nanotubes. *AIP Conference Proceedings* **2001**, *590*,107–112.

28. Tombler, T.W.; Zhou, C.; Alexseyev, L.; Kong, J.; Dai, H.; Liu, L.; Wu, S.Y. Reversible electromechanical characteristics of carbon nanotubes under local-probe manipulation. *Nature* **2000**, *405*, 769–772.

29. Jeon, E.K.; Park, C.H.; Lee, J.A.; Kim, M.S.; Lee, K.C.; So, H.M.; Ahn, C.; Kong, K.-J.; Kim, J.-J.; Lee, J.-O. Electromechanical properties of single-walled carbon nanotube devices on micromachined cantilevers. *J. Micromech. Microeng.* **2012**, *22*, 115010.

30. Cullinan, M.A.; Martin, L. Culpepper. Carbon nanotubes as piezoresistive microelectromechanical sensors: Theory and experiment. *Phys. Rev. B* **2010**, *82*, 115428.

31. Hu, N.; Karube, Y.; Arai, M.; Watanabe, T.; Yan, C.; Li, Y.; Liu, Y.L.; Fukunaga, H. Investigation on sensitivity of a polymer/carbon nanotube composite strain sensor. *Carbon* **2010**, *48*, 680–687.

32. De Vivo, B.; Lamberti, P.; Spinelli, G.; Tucci, V. Numerical investigation on the influence factors of the electrical properties of carbon nanotubes-filled composites. *J. Appl. Phys.* **2013**, *113*, 244301.

33. Wang, Z.; Ye, X. A numerical investigation on piezoresistive behaviour of carbon nanotube/polymer composites: Mechnism and optimizing principle. *Nanotechnology* **2013**, *24*, 265704.

34. Pereira, L.F.C.; Ferreira, M.S. Electronic transport on carbon nanotube networks: A multiscale computational approach. *Nano Commun. Netw.* **2011**, *2*, 25–28.

35. Rausch, J.; Mädler, E. Health monitoring in continuous glass fiber reinforced thermoplastics: Tailored sensitivity and cyclic loading of CNT-based interphase sensors. *Compos. Sci. Technol.* **2010**, *70*, 2023–2030.

36. Bauhofer, W.; Kovacs, J.Z. A review and analysis of electrical percolation in carbon nanotube polymer composites. *Compos. Sci. Technol.* **2009**, *69,* 1486–1498.

37. Moniruzzaman, M.; Winey, K.I. Polymer nanocomposites containing carbon nanotubes. *Macromolecules* **2006**, *39*, 5194–5205.

38. Gerlach, C.; Kanoun, O. Printable piezoresistive carbon nanotube-elastomer for pressure sensors, *Tech. Mess.* **2013**, *80*, 9–15.

39. Zeng, Y.L.; Huang, Y.F.; Jiang, J.H.; Zhang, X.B.; Tang, C.R.; Shen, G.L. Functionalization of multiwalled carbon nanotubes with poly(amidoamine) dendrimer for mediatorfree glucose biosensor. *Electrochem. Commun.* **2007**, *9*, 185–190.

40. Deutscher, G. Disordered systems and localization. In *Percolation and Superconductivity*; Goldman, A.M., Wolf, S.A., Eds.; Plenum Press: New York, NY, USA, 1984; pp. 95–113.

41. Kaempgen, M Eigenschaften und Anwendungen von Netzwerken aus Kohlenstoff-Nanoröhren. Ph.D. Dissertation, Online Stuttgart University Library, Stuttgart, Germany, 2006.
42. Wang, P.; Geng, S.; Ding, T. Effects of carboxyl radical on electrical resistance of multi-walled carbon nanotube filled silicone rubber composite under pressure. *Compos. Sci. Technol.* **2010**, *70*, 1571–1573.
43. Alamusi; Hu, N.; Fukunaga, H.; Atobe, S.; Lui, Y.; Li, J. Piezoresistive strain sensors made from carbon nanotubes based polymer nanocomposites. *Sensors* **2011**, *11*, 10691–10723.
44. Grossiord, N.; Loos, J.; van Laake, L.; Maugey, M.; Zakri, C.; Koning, C.E.; Hart, A.J. High-conductivity polymer nanocomposites obtained by tailoring the characteristics of carbon nanotube fillers. *Adv. Funct. Mater.* **2008**, *18*, 3226–3234.
45. Oliva-Avilés, A.I.; Avilés, F.; Sosa, V. Electrical and piezoresistive properties of multi-walled carbon nanotube/polymer composite films aligned by an electric field. *Carbon* **2011**, *49*, 2989–2997.
46. Girifalco, L.A.; Hodak, M.; Lee, R.S. Carbon nanotubes, buckyballs, ropes, and a universal graphitic potential. *Phys. Rev. B* **2000**, *62*, 13104.
47. Takahashi, T.; Takei, K.; Gillies, A.G.; Fearing, R.S.; Javey, A. Carbon nanotube active-matrix backplanes for conformal electronics and sensors. *Nano Lett.* **2011**, *11*, 5408–5413.
48. Kong, J.; Chapline, M.G.; Dai, H. Functionalized carbon nanotubes for molecular hydrogen sensors. *Adv. Mater.* **2001**, *13*, 1384–1386.
49. Mubeen, S.; Zhang, T.; Yoo, B.; Deshusses, M.A.; Myung, N.V. Palladium nanoparticles decorated single-walled carbon nanotube hydrogen sensor. *J. Phys. Chem. C* **2007**, *111*, 6321–6327.
50. Sun, L.; Warren, G.L.; O'Reilly, J.Y.; Everett, W.N.; Lee, S.M.; Davis, D. Mechanical properties of surface-functionalized SWCNT/epoxy composites. *Carbon* **2008**, *46*, 320–328.
51. Coleman, J.N.; Khan, U.; Blau, W.J.; Gun'ko, Y.K. Small but strong: A review of the mechanical properties of carbon nanotube–polymer composites. *Carbon* **2006**, *44*, 1624–1652.
52. Breuer, O.; Sundararaj, U. Big returns from small fibers: A review of polymer/carbon nanotube composites. *Polym. Compos.* **2004**, *25*, 630–645.
53. Vaisman, L.; Marom, G.; Wagner, H.D. Dispersions of surface modified carbon nanotubes in water-soluble and water-insoluble polymers. *Adv. Funct. Mater.* **2006**, *16*, 357–363.
54. O'Connell, M.J.; Bachilo, S.M.; Huffman, C.B.; Moore, V.C.; Strano, M.S.; Haroz, E.H.; Rialon, K.L.; Boul, P.J.; Noon, W.H.; Kittrell, C.; *et al.* Band Gap Fluorescence from individual single-walled carbon nanotubes. *Science* **2002**, *297*, 593–596.
55. Islam, M.F.; Roja, E.; Bergey, D.M.; Johnson, A.T.; Yodh, A.G. High weight fraction surfactant solubilization of single-wall carbon nanotubes in water. *Nano Lett.* **2003**, *3*, 269–273.
56. Moore, V.C.; Strano, M.S.; Haroz, E.H.; Hauge, R.H.; Smalley, R.E. Individually suspended single-walled carbon nanotubes in various surfactants. *Nano Lett.* **2003**, *3*, 1379–1382.
57. Whitsitt, E.A.; Barron, A.R. Silica coated single walled carbon nanotubes. *Nano Lett.* **2003**, *3*, 775–778.
58. Cooper, C.A.; Ravich, D.; Lips, D.; Mayer, J.; Wagner, H.D. Distribution and alignment of carbon nanotubes and nanofibrils in a polymer matrix. *Compos. Sci. Technol.* **2002**, *62*, 1105–1112.

59. Yurekli, K.; Mitchell, C.A.; Krishnamoorti, R. Small-angle neutron scattering from surfactant-assisted aqueous dispersions of carbon nanotubes. *J. Am. Chem. Soc.* **2004**, *126*, 9902–9903.

60. Kim, S.T.; Choi, H.J.; Hong, S.M. Bulk polymerized polystyrene in the presence of multiwalled carbon nanotubes. *Coll. Polym. Sci.* **2007**, *285*, 593–598.

61. Jia, Z.; Wang, Z.; Xu, C.; Liang, J.; Wie, B.; Wu, D. Study on poly(methylmethacrylate): Carbon nanotube composites. *Mater. Sci. Eng. A* **1999**, *271*, 395–400.

62. Zhang, Q.H.; Chen, D.J. Percolation threshold and morphology of composites of conducting carbon black/polypropylene/EVA. *J. Mater. Sci.* **2004**, *39*, 1751–1757.

63. Hill, D.E.; Rao, A.M.; Allard, L.F.; Sun, Y.P. Functionalization of carbon nanotubes with polystyrene. *Macromolecules* **2002**, *35*, 9466–9471.

64. Wardle, B. L.; Saito, D. S.; Garcia, E. J.; Hart, A. J.; de Villoria, R. G. and Verploegen, E. A. Fabrication and Characterization of Ultrahigh-Volume- Fraction Aligned Carbon Nanotube–Polymer Composites. *Adv. Mater.*, **2008**, *20*, 2707-2014.

65. Mureau, N.; Mendoza, E.; Silva, S. R. P.; Hoettges, K. F. and Hughes M. P. In Situ and Real Time Determination of Metallic and Semiconducting Single-Walled Carbon Nanotubes in Suspension via Dielectrophoresis. *Appl. Phys. Lett.*, **2006**, *88*, 243109.

66. Steinert, B. W. and Dean, D. R. Magnetic field alignment and electrical properties of solution cast PET–carbon nanotube composite films. *Polymer*, **2009**, *50*, 898-904.

67. Cheng, Q.; Bao, J.; Park, J.; Liang, Z.; Zhang, C. and Wang, B. High Mechanical Performance Composite Conductor: Multi-Walled Carbon Nanotube Sheet/Bismaleimide Nanocomposites. *Adv. Funct. Mater.*, **2009**, *19*, 3219.

68. Vigolo, B.; Penicaud, A.; Coulon, C.; Sauder, C.; Pailler, R.; Journet, C.; Bernier, P. and Poulin, P. Macroscopic fibers and ribbons of orientated carbon nanotubes. *Science*, **2000**, *290*, 1331-1334.

69. Zhang, X.; Liu, T.; Sreekumar, T. V.; Kumar, S.; Hu, X. and Smith, K. Gel spinning of PVA/SWNT composite fiber. *Polymer*, **2004**, *45*, 8801-8807.

70. Sreekumar, T. V.; Liu, T.; Min, B. G.; Guo, H.; Kumar, S.; Hauge, R. H. and Smalley R. E. SWNT/PAN Composite Fibers. *Adv. Mater.*, **2004**, *16*, 58-61.

71. Ko, F.; Gogotsi, Y.; Ali, A.; Naguib, N.; Ye, H.; Yang, G. L.; Li, C. and Wilis, P. Electrospinning of continuous carbon nanotube-filled nanofiber yarns. *Adv. Mater.*, **2003**, *15*, 1161-1165.

72. Bu, L.; Steiz, J.; Kanoun, O. Influence of processing parameters on properties of strain sensors based on carbon nanotube films. In Proceedings of the 7th International Multi-Conference on Systems, Signals and Devices—Sensors, Circuits & Instrumentation Systems, Amman, Jordanien 27–30 June 2010.

73. Chen, W.; McCarthy, T. Layer-by-layer deposition: A tool for polymer surface modification. *Macromolecules* **1997**, *30*, 78–86.

74. Dongsik, Y.; Shiratori, S.Y.; Rubner, M.F. Controlling bilayer composition and surface wettability of sequentially adsorbed multilayers of weak polyelectrolytes. *Macromolecules* **1998**, *30*, 4309–4318.

75. Shiratori, S.S.; Rubner, M. pH-Dependent thickness behavior of sequentially adsorbed layers of weak polyelectrolytes. *Macromolecules* **2000**, *30*, 4213–4219.

76. Kolasinska, M.; Krastev, R.; Gutberlet, T.; Warszynski, P. Layer-by-layer deposition of polyelectrolytes. Dipping *versus* spraying. *Langmuir* **2009**, *25*, 1224–1232.

77. Mendelsohn, J.D.; Barrett, C.J.; Chan, V.V.; Pal, A.J.; Mayes, A.M.; Rubner, M.F. Fabrication of microporous thin films from polyelectrolyte multilayers. *Langmuir* **2000**, *16*, 5017–5023.

78. Brown, J.J.; Hall, R.A.; Kladitis, P.E.; George, S.M.; Bright, V.M. Molecular layer deposition on carbon nanotubes. *ACS Nano* **2013**, *7*, 7812–7823.

79. Kordás, K.; Mustonen, T.; Tóth, G.; Jantunen, H.; Lajunen, M.; Soldano, C.; Talapatra, S.; Kar, S.; Vajtai, R.; Ajayan, P.M. Inkjet printing of electrically conductive patterns of carbon nanotubes. *Small* **2006**, *2*, 1021–1025.

80. Song, J.W.; Kim, J.; Yoon, Y.H.; Choi, B.S.; Kim, J.H.; Han, C.S. Inkjet pring of single-walled carbon nanotubes and electrical characterization of the line pattern. *Nanotechnology* **2008**, *19*, 095702.

81. Denneulin, A.; Bras, J.; Blayo, A.; Khelifi, B.; Roussel-Dherbey, F.; Neuman, C. The influence of carbon nanotubes in inkjet printing of conductive polymer suspensions. *Nanotechnology* **2009**, *20*, 385701.

82. Jones, C.S.; Lu, X.; Renn, M.; Stroder, M.; Shih, W.S. Aerosol-jet-printed, high-speed, flexible thin-film transistor made using single-walled carbon nanotube solution. *Microelectron. Eng.* **2010**, *87*, 434–437.

83. Vaillancourt, J.; Zhang, H.; Vasinajindakaw, P.; Haitou, X.; Lu, X.; Han, X.; Janzen, D.C.; Shih, W.S.; Jones, C.S.; Stroder, M.; *et al.* All ink-jet-printed carbon nanotube thin-film transistor on a polyimide substrate with an ultrahigh operating frequency of over 5 GHz. *Appl. Phys. Lett.* **2008**, *93*, 243301.

84. Ha, M.; Xia, Y.; Green, A.A.; Zhang, W.; Renn, M.J.; Kim, C.H.; Hersam, M.C.; Frisbie, C.D. Printed, sub-3V digital circuits on plastic from aqueous carbon nanotube inks. *ACS Nano* **2010**, *4*, 4388–4395.

85. Li, J.; Lei, W.; Zhang, X; Zhou, X.; Wang, Q.; Zhang, Y.; Wang, B. Field emission characteristic of screen-printed carbon nanotube cathode. *Appl. Surf. Sci.* **2003**, *220*, 96–104.

86. Liu, C.X.; Choi, J.W. Patterning conductive PDMS nanocomposite in an elastomer using microcontact printing. *J. Micromech. Microeng.* **2009**, *19*, 085019.

87. Jung, M.; Kim, J.; Noh, J.; Lim, N.; Lim, C.; Lee, G.; Kim, J.; Kang, H.; Jung, K.; Leonard, A.D.; *et al.* All-printed and roll-to-roll-printable13.56-MHz-operated 1-bit RF tag on plastic foils. *IEEE Trans. Electron Devices* **2010**, *57*, 571–580.

88. Chen, P.; Fu, Y.; Aminirad, R.; Wang, C.; Zhang, J.; Wang, K.; Galatsis, K.; Zhou, C. Fully printed separated carbon nanotube thin film transistor circuits and its application in organic light emitting diode control. *Nano Lett.* **2011**, *11*, 5301–5308.

89. Gelinck, G.H.; Huitema, H.E.A.; van Veenendaal, E.; Cantatore, E.; Schrijnemakers, L.; van der Putten, J.B.P.H.; Geuns, T.C.T.; Beenhakkers, M.; Giesbers, J.B.; Huisman, B.H.; *et al.* Flexible ative-matrix displays and shift registers based on solution-processed organic transistors. *Nat. Mater.* **2004**, *3*, 106–110.

90. Huang, L.; White, B.; Sfeir, M.Y.; Huang, M.; Huang, H.X.; Wind, S.; Hone, J.; O'Brien, S. Cobalt ultrathin film catalyzed ethanol chemical vapor deposition of single-walled carbon nanotubes. *J. Phys. Chem. B* **2006**, *110*, 11103–11109.

91. Ryu, K.; Badmaev, A.; Wang, C.; Lin, A.; Patil, N.; Gomez, L.; Kumar, A.; Mitra, S.; Wong, H.S.P.; Zhou, C. CMOS-analogous wafer-scale nanotube-on-insulator approach for submicrometer devices and integrated circuits using aligned nanotubes. *Nano Lett.* **2008**, *9*, 189–197.

92. Hong, S.W.; Banks, T.; Rogers, J.A. Improved density in aligned arrays of single-walled carbon nanotubes by sequential chemical vapor deposition on quartz. *Adv. Mater.* **2010**, *22*, 1826–1830.

93. Zhou, W.; Ding, L.; Yang, S.; Liu, J. Synthesis of high-density, large-diameter, and aligned single-walled carbon nanotubes by multiple-cycle growth methods. *ACS Nano* **2011**, *5*, 3849–3857.

94. Collins, P.C.; Arnold, M.S.; Avouris, P. Engineering carbon nanotubes and nanotube circuits using electrical breakdown *Science* **2001**, *292*, 706–709.

95. Zhou, Y.; Gaur, A.; Hur, S.H.; Kocabas, C.; Meitl, M.A.; Shim, M.; Rogers, J.A. P-channel, n-channel thin film transistors and p-n diodes based on single wall carbon nanotube networks. *Nano Lett.* **2004**, *4*, 2031–2035.

96. Hellstrom, S.L.; Lee, H.W.; Bao, Z. Polymer–assisted direct deposition of uniform carbon nanotube bundle networks for high performance transparent electrodes *ACS Nano* **2009**, *3*, 1423–1430.

97. Jo, J.W.; Jung, J.W.; Lee, J.U.; Jo, W.H. Fabrication of highly conductive and transparent thin films from single-walled carbon nanotubes unsing a new non-ionic surfactant via spin coating. *ACS Nano* **2010**, *4*, 5382–5388.

98. Kim, S.; Yonghyuk, Y.; Wang, X.; Bradley, D.D.C.; Lee, S.; de Mello, J.C. Spin- and spray-deposited single-walled carbon-nanotube electrodes for organic solar cells. *Adv. Funct. Mater.* **2010**, *20*, 2310–2316.

99. Tenent, R.C.; Barnes, T.M.; Bergeson, J.D.; Ferguson, A.J.; To, B.; Geddvilas, L.M.; Hebben, M.J.; Blackburn, J.L. Ultra smooth, large-area, high-uniformity, conductive transparent single-walled-carbon-nanotube films for photovoltaics produced by ultrasonic spraying. *Adv. Mater.* **2009**, *21*, 3210–3216.

100. Ghahremanpour, M.; Sägebarth, J.; Weis, D.G.; Sandmaier, H. Strain sensitive films with spray-coated carbon nanotubes. In Proceedings of the Eurosensors XXII, CD-ROM, Dresden, Germany, 7–10 September 2008; pp. 656–659.

101. Lee, D.; Hong, H.P.; Li, J.C.; Park, C.W.; Min, M.K. Microfabrication and characterization of spray-coated single-wall carbon nanotube film strain gauges. *Nanotechnology* **2011**, *22*, 455301.

102. Wu, Z.; Chen, Z.; Du, X.; Logan, J.M.; Sippel, J.; Nikolou, M.; Kamaras, K.; Reynolds, J.R.; Tanner, T.B.; Hebard, A.F.; *et al.* Transparent, conductive carbon nanotube films. *Science* **2004**, *305*, 1273–1276.

103. Zhou, Y.; Hu, L.; Grüner, G. A method of printing carbon nanotube thin film. *Appl. Phys. Lett.* **2006**, *88*, 123109.

104. Dharap, P.; Li, Z.; Nagarajaiah, S.; Barrera, E.V. Nanotube film based on single-wall carbon nanotubes for strain sensing. *Nanotechnology* **2004**, *15*, 379–382.

105. Celzard, A.; McRae, E.; Deleuze, C.; Dufort, M.; Furdin, G.; Marêché, J.F. Critical concentration on percolating systems containing a high-aspect-ratio filler. *Phys. Rev. B* **1996**, *53*, 6209–6214.

106. Simmons, J.G. Generalized formula for the electric tunnel effect between similar electrodes separated by a thin insulating film. *J. Appl. Phys.* **1963**, *34*, 1793–1803.

107. Hu, N.; Karube, Y.; Yan, C.; Masuda, Z.; Fukunaga, H. Tunneling effect in polymer/carbon nanotube nanocomposite strain sensor. *Acta Mater.* **2008**, *56*, 2929–2936.

108. Bae, D.J.; Kim, K.S.; Park, Y.S.; Suh, E.K.; An, K.H.; Moon, J.M.; Lim, S.C.; Park, S.H.; Jeong, Y.H.; Lee, Y.H. Transport phenomena in an anisotropically aligned single-wall carbon nanotube film. *Phys. Rev. B* **2001**, *64*, 233401.

109. Theodosiou, T.C.; Saravanos, D.A. Numerical investigation of mechanisms affecting the piezoresistive properties of CNT-doped polymers using multi-scale models. *Compos. Sci. Technol.* **2010**, *70*, 1312–1320.

110. Liu, Y.L.; Hu, N. Numerical simulations on piezoresistivity of CNT/polymer based nanocomposites. *Comput. Mater. Contin.* **2010**, *20*, 101–118.

111. Li, Z.; Dharap, P.; Nagarajaiah, S.; Barrera, E.V.; Kim, J.D. Carbon nanotube film sensors. *Adv. Mater.* **2004**, *16*, 640–643.

112. Obitayo, W. and Liu, T. A review: Carbon nanotube-based piezoresistive strain sensors. *J. Sensors*, **2012**.

113. Li, X.; Levy, C. and Elaadil, L. Multiwalled carbon nanotube film for strain sensing. *Nanotechnology*, **2008**, 19(4), 045501.

114. Vemuru, S. M.; Wahi, R.; Nagarajaiah, S. and Ajayan, P. M. Strain sensing using a multiwalled carbon nanotube film. *J. Strain Anal. Eng. Design*, **2009**, 44(7), 555-562.

115. Dinh, T. N.; Sowade, E.; Arreba, A.; Belau, R.; Blaudeck, T.; Baumann, R. R. and Kanoun, O. Performance of liquid-deposited multiwalled carbon nanotube films under strain, *Printing Future Da*ys, **2011**, 109-115.

116. Wan-Lu, W.; Ke-Jun, L.; Yong, L. and Yong-Tian, W. Piezoresistive effect of doped carbon nanotube/cellulose films. *Chin. Phys. Lett.*, **2003**, 20(9), 1544

117. Dinh, T. N.; Steitz, J.; Bu, L. and Kanoun, O. Influence of the composition of MWCNTs layers on the properties of strain gauges, 9th IEEE Conference on Nanotechnology, **2009**, 477 - 480.

118. Yang, L.; Anantram, M. P.; Han, J. and Lu, J. P. Band-gap change of carbon nanotubes: Effect of small uniaxial and torsional strain. *Phys. Rev. B*, **1999**, 60(19), 13874.

119. Yang, L. and Han, J. Electronic structure of deformed carbon nanotubes. *Phys. Rev. Lett.*, **2000**, 85(1), 154.

120. Heyd, R.; Charlier, A. and McRae, E. Uniaxial-stress effects on the electronic properties of carbon nanotubes. *Phys. Rev. B*, **1997**, 55(11), 6820.

121. Hone, J.; Llaguno , M. C.; Nemes, N. M.; Johnson, A. T.; Fischer, J. E.; Walters, D. A. Casavant, M. J.; Schmidt, J. and R. E. Smalley. Electrical and thermal transport properties of magnetically aligned single wall carbon nanotube films. *Appl. Phys. Lett.* 77, **2000**, 5, 666-668.

122. Barberio, M.; Camarca, M.; Barone, P.; Bonanno, A.; Oliva, A. and Xu, F. Electric resistivity of multi-walled carbon nanotubes at high temperatures. *Surf. Sci.*, **2007**, 601(13), 2814-2818.

123. Yin, G.; Hu, N.; Karube, Y.; Liu, Y.; Li, Y. and Fukunaga, H. A carbon nanotube/polymer strain sensor with linear and anti-symmetric piezoresistivity. *Compos. Mater.* **2011**, *45*, 1315–1323.

124. Loh, K., Hou, T., Lynch, J., and Kotov, N. Nanotube-based Sensing Skins for Crack Detection and Impact Monitoring of Structures, Proceedings of the 6th International Workshop on Structural Health Monitoring, Stanford, CA, September 11-13, 2007.

125. Ramasubramaniam, R.; Chen, J. Homogeneous carbon nanotube/polymer composites for electrical applications. *Appl. Phys. Lett.* **2002**, *83*, 2928–2930.

126. Mechrez, G.; Suckeveriene, R.Y.; Zelikman, E.; Rosen, J.; Ariel-Sternberg, N.; Cohen, R.; Narkis, M.; Segal, E. Highly-tunable polymer/carbon nanotubes systems: Preserving dispersion architecture in solid composites via rapid microfiltration. *ACS Macro Lett.* **2012**, *1*, 848–852.

127. Chen, M.; Tao, T.; Zhang, L.; Gao, W.; Li, C. Highly conductive and stretchable polymer composites based on graphene/MWCNT network. *Chem. Commun.* **2013**, *49*, 1612–1614.

128. Loh, K.J.; Lynch, J.P.; Shim, B.S.; Kotov, N.A. Tailoring piezoresistive sensitivity of multilayer carbon nanotube composite strain sensors. *J. Intell. Mater. Syst. Struct.* **2008**, *19*, 747–764.

129. Loh, K.J.; Kim, J.; Lynch, J.P.; Kam, N.W.S.; Kotov, N.A. Multifunctional layer-by-layer carbon nanotube–polyelectrolyte thin films for strain and corrosion sensing. *Smart Mater. Struct.* **2007**, *16*, 429–438.

130. Pham, G.T.; Park, Y.-B.; Liang, Z.; Zhang, C.; Wang, B. Processing and modeling of conductive thermoplastic/carbon nanotube films for strain sensing. *Compos. Part B* **2008**, *39*, 209–216.

131. Park, M.; Kim, H.; Youngblood, J.P. Strain-dependent electrical resistance of multi-walled carbon nanotubes/polymer composite films. *Nanotechnology* **2008**, *19*, 055705.

132. Wichmann, M.H.G.; Buschhorn, S.T.; Böger, L.; Adelung, R.; Schulte, K. Direction sensitive bending sensors based on multi-wall carbon nanotube/epoxy nanocomposites. *Nanotechnology* **2008**, *19*, 475503.

133. Wichmann, M.H.G.; Buschhorn, S.T.; Gehrmann, J.; Schulte, K. Piezoresistive response of epoxy composites with carbon nanoparticles under tensile load. *Phys. Rev. B* **2009**, *80*, 245437.

134. Hu, N.; Itoi, T.; Akagi, T.; Kojima, T.; Xue, J.; Yan, C.; Atobe, S.; Fukunaga, S.; Yuan, W.; Ning, H.; *et al.* Ultrasensitive strain sensors made from metal-coated carbon naofiller/epoxy composites. *Carbon* **2013**, *51*, 202–212.

135. Zhao, H.; Zhang, Y.; Bradford, P. D.; Zhou, Q.; Jia, Q.; Yuan, F. G. and Zhu, Y. Carbon nanotube yarn strain sensors. *Nanotechnology*, **2010**, 21(30), 305502.

136. Shang, Y.; Li, Y.; He, X.; Zhang, L.; Li, Z.; Li, P.; Shi, E.; Wu, S. and Cao, A. Elastic carbon nanotube straight yarns embedded with helical loops. *Nanoscale* **2013**, 5(6), 2403-2410.

137. Li, Y.; Shang, Y.; He, X.; Peng Q.; Du, S.; Shi E.; Wu, S.; Li, Z. and Cao, A. Overtwisted, Resolvable Carbon Nanotube Yarn Entanglement as Strain Sensors and Rotational Actuators. *ACS Nano* **2013**, 7 (9), 8128–8135

138. Kahng, S. K.; Gates T. S.; Jefferson, G.D. Strain and Temperature Sensing Properties of Multiwalled Carbon. Nanotube Yarn Composites. *NASA Technical Report* **2008**.

139. Carmen, K. M.; Fung, M.; Zhang, Q. H.; Zaili, D. and Wen, J. L. Fabrication of CNT-Based MEMS Piezoresistive Pressure Sensors Using DEP Nanoassembly. *5th IEEE Conference on Nanotechnology* **2005**, *1*, 199 – 202.

140. Qian, K.; Chen, T.; Yan, B.; Lin, Y.; Xu, D.; Sun, Z. and Cai, B. Research on carbon nanotube array field emission pressure sensors. *Electronics Lett.* **2005**, 41, 824 – 825.

141. Gau, C.; Ko, H. S. and Chen, H.T. Piezoresistive characteristics of MWNT nanocomposites and fabrication as a polymer pressure sensor. *Nanotechnology* **2009**, 20, 185503.

142. Ko, H. S.; Liu, C. W. and Gau C. A novel fabrication for pressure sensor with polymer material and evaluation of its performance, *J. Micromech. Microeng* **2007**, 17, 1640–1648.

143. Wang, P.; Geng, S.; Ding, T. Effects of carboxyl radical on electrical resistance of multi-walled carbon nanotube filled silicone rubber composite under pressure. *Compos. Sci. Technol.* **2010**, *70*, 1571-1573.

144. Mohiuddin, M. and Van Hoa, S. Electrical resistance of CNT-PEEK composites under compression at different temperatures, *Nanoscale Research Letters* **2011**, 6, 419-424.

145. Yilmazoglu, O.; Popp, A.; Pavlidis, D.; Schneider, J. J.; Garth, D.; Schuttler, F. and Battenberg, G.Vertically aligned multiwalled carbon nanotubes for pressure, tactile and vibration sensing, *Nanotechnology* **2012**, 23, . 085501.

146. Taak, S.; Rajabali, S.; Darbari, S. and Mohajerzadeh, S. High sensitive/wide dynamic range, field emission pressure sensor based on fully embedded CNTs. *J. Phys. D: Appl. Phys.* **2014** 47, 045302.

147. Haniff, M. A. S. M.; Lee, H. W.; Bien, D. C. S.; The, A. S. and Azid, I. A. Highly sensitive integrated pressure sensor with horizontally oriented carbon nanotube network. *Nanoscale Research Letters* **2014**, 9, 49.

148. Bsoul, A.; Mohamed Ali M. S. and Takahata K. Piezoresistive pressure sensor using vertically aligned carbon-nanotube forests. *Electronics Lett.* **2011**, 47, 807-808.

149. Park, C. S.; Kang, B. S.; Lee, D. W. and Choi, Y. S. Single carbon fiber as a sensing element in pressure sensors. *Appl. Phys. Lett.* **2006**, 89, 223516.

150. Su, C. C.; Li, C. H.; Chang, N. K.; Gao, F. and Chang, S. H. Fabrication of high sensitivity carbon microcoil pressure sensors. *Sensors* **2012**, 12, 10034–10041.

151. Lim, C.; Lee, K.; Choi, E.; Kim, A.; Kim, J. and Lee, S. B. Effect of nanoscale surface texture on the contact-pressure-dependent conduction characteristics of a carbon-nanotube thin-film tactile pressure sensor. *J. Korean Phys. Soc.* **2011**, 58, 72–76.

152. So, H.-M.; Sim, J. W.; Kwon, J.; Yun, J.; Baik, S. and Chang, W. S. Carbon nanotube based pressure sensor for flexible electronics, Materials Research Bulletin **2013**, 48, 5036–5039.

153. Sepúlveda, A.T.; Fachin, F.; Guzmán de Villoria, R.; Wardle, B. L.; Viana, J. C.; Pontes, A. J. and Rocha, L. A. Nanocomposite flexible pressure sensor for biomedical applications, *Procedia Engineering*, **2011**, 25, 140-143.

154. Shindo, Y.; Kuronuma, Y., Takeda, T.; Narita, F. and Fu, S. Y. Electrical resistance change and crack behavior in carbon nanotube/polymer composites under tensile loading, *Composites Part B: Engineering*, **2012**, 43, 39-43.

155. Inam, F.; Bhat, B.; Vo, T. and Daoush, W. Structural health monitoring capabilities in ceramic–carbon nanocomposites, *Ceramics International*, **2014**, 40, 3793-3798.

156. Loh, K.; Lynch, J.; Kotov, N. Passive wireless strain and ph sensing using carbon nanotube-gold nanocomposite thin films. Proc. SPIE 2007, 652919, 1–12.

157. Benchirouf, A.; Sowade, E.; Blaudeck, T.; Kanoun, O. and Baumann, R. R. Design and characterization of inkjet-printed passive wireless strain sensor based on carbon nanotubes, *Printing Future Days*, **2011**, 109-115.

158. Tang, Q. Y.; Pan, Y. M.; Chan, Y. C. and Leung, K. W. Frequency-tunable soft composite antennas for wireless sensing, *Sensors and Actuators A*, **2012**, *179*, 2012, 137– 145.

159. Tata, U.; Cao, H. and Landge, V. Wireless strain sensor based on amorphous carbon for human-motion detection, 2013 IEEE Topical Conference on Biomedical Wireless Technologies, Networks, and Sensing Systems.